UNIVERSIDADE DE BRASÍLIA

FACULDADE DE CIÊNCIAS DA SAÚDE

ANA LUIZA LIMA DO NASCIMENTO

APPLICATION OF OSCILLATORY SHEAR RHEOLOGY FOR THE DEVELOPMENT OF PHARMACEUTICAL SYSTEMS BY HOT-MELT EXTRUSION AND FDM 3D PRINTING

BRASÍLIA

2021

UNIVERSIDADE DE BRASÍLIA

FACULDADE DE CIÊNCIAS DA SAÚDE

ANA LUIZA LIMA DO NASCIMENTO

APPLICATION OF OSCILLATORY SHEAR RHEOLOGY FOR THE DEVELOPMENT OF PHARMACEUTICAL SYSTEMS BY HOT-MELT EXTRUSION AND FDM 3D PRINTING

> Trabalho de Conclusão de Curso apresentado à Universidade de Brasília como requisito para obtenção de grau Farmacêutico.
> Orientador: Marcílio Sérgio Soares da Cunha Filho

BRASÍLIA

2021

DEDICATÓRIA

Ao meu avô, Eduardo, por seu amor e carinho e por todos os sonhos que um dia sonhou para mim.

AGRADECIMENTOS

RESUMO

Os avanços tecnológicos recentes apontam que o futuro do segmento farmacêutico deverá envolver o uso inovador dos processos de *hot-melt extrusion* e impressão 3D por modelagem de deposição fundida. Com a finalidade de contribuir no desenvolvimento de medicamentos elaborados através dessas técnicas emergentes de processamento, o objetivo desse trabalho foi avaliar o potencial de aplicação da reologia oscilatória como uma ferramenta analítica capaz de auxiliar a elaboração de medicamentos 3D que cumpram com os requisitos de qualidade preconizados. Para isso, conceitos gerais de reologia, reometria, viscoelasticidade e metodologias rotacionais e oscilatórias foram resumidos e esquematizados. A aplicação teórica desses conceitos para técnicas de extrusão e impressão 3D também foi apresentada, incluindo as vantagens e limitações da reologia para a caracterização de materiais sólidos. A segunda etapa do trabalho consistiu em um estudo experimental, no qual a reologia de cisalhamento oscilatório foi avaliada como ferramenta de controle em processo na elaboração de comprimidos por impressão 3D. Para esse fim, filamentos de álcool polivinílico foram produzidos com diferentes concentrações de plastificante (glicerina) e posteriormente impressos em duas impressoras 3D FDM diferentes. O aumento na proporção de plastificante ($\geq$ 30%) elevou a deformação viscosa, resultando em materiais muito flexíveis que são inadequados para impressão. Por outro lado, os filamentos com 10 – 20% de plastificante apresentaram viscosidade adequada (perto de 0,8 kPa.s), diâmetro homogêneo e resistência suficiente à força extensional, produzindo filamentos que permitem serem tracionados, e que são capazes de fluir através do bico e construir estruturas 3D camada por camada. Portanto, a avaliação da viscoelasticidade através de reologia oscilatória pode antecipar problemas na capacidade de impressão dos filamentos, identificando possíveis erros de impressão e instabilidades nos medicamentos 3D.

Palavras-chave: reologia; polímeros farmacêuticos; reometria; impressão tridimensional; viscoelasticidade.

ABSTRACT

Recent technological advances indicate that the future of pharmaceutical industry will involve the innovative use of hot-melt extrusion and fused deposition modeling 3D printing. Claiming to assist to the development of drugs produced through these emerging processing techniques, the objective of this work was to evaluate the potential application of oscillatory rheology as an analytical tool capable of contributing to the development of 3D drugs that meet the recommended quality standards requirements. For this, general concepts of rheology, rheometry, viscoelasticity and rotational and oscillatory methodologies were summarized and outlined. The theoretical application of these concepts to extrusion and 3D printing techniques was also developed, including the advantages and limitations of rheology for the characterization of solid materials. The second stage of the work consisted of an experimental study in which oscillatory shear rheology was evaluated as an in-process control tool in the preparation of tablets by 3D printing. For this purpose, polyvinyl alcohol filaments were produced using different plasticizer concentrations (glycerin) and subsequently printed on two different 3D printers. The increase in plasticizer ratio ($\geq 30\%$) enhanced viscous deformation, resulting in too flexible materials that are inappropriate for printing. On the other hand, filaments with 10-20% of plasticizer presented suitable viscosity (close to 0.8 kPa.s), homogeneous diameter and sufficient resistance to extensional force, producing filaments that can be pulled by the gear, and that are able to flow through the nozzle and build 3D structures layer by layer. Therefore, viscoelasticity and tensile strength measurements could anticipate problems in filaments printability, identifying possible printing errors, and instabilities of 3D medicines.

Keywords: rheology; pharmaceutical polymer; rheometry; three-dimensional printing; viscoelasticity.

LIST OF FIGURES

LIST OF TABLES

LIST OF ABREVIATIONS

3D	Three-dimensional
3D-FDM	Fused deposition modeling 3D printing
3DP	3D printing
A	Area
DHR	Discovery Series Hybrid Rheometer
DSC	Differential mscanning calorimetry
DTG	Derivative Thermogravimetry
F	Force
G'	Elastic modulus/Storage modulus
G"	Viscous modulus/Loss modulus
G*	Complex modulus
GLY	Glycerin
HME	Hot-melt extrusion
LAOS	Large amplitude oscillatory shear
LVR	Linear viscoelastic response
p	Level of significance
PVA	Polyvinyl alcohol
RPM	Rotation per minute
S	Deflection path
SAOS	Small amplitude oscillatory shear
Tan δ	Tangent of phase angle delta (δ)
TGA	Thermogravimetric analysis
v	Speed
γ	Strain
$\dot{\gamma}$	Shear rate
δ	Phase angle delta
η	Viscosity
η*	Complex viscosity
ω	Angular frequency
τ	shear stress

SUMMARY

CHAPTER 1 - BASIC CONCEPTS ON RHEOLOGY

To provide theoretical support for the development and evaluation of rheological analysis, this part of the work aims to assemble basic concepts of rheology and rheometry, including the main methodological variables currently used (rotation and oscillation) as well as the concept that guides rheological understanding, viscoelasticity.

1.1 Rheology and rheometry

Rheology is defined as the study of stress-deformation relationships, referring to material's flow when stressed (GUZMÁN et al., 2018). Therefore, rheology can describe the deformation behavior of all kinds of materials, from the flow of liquids to the deformation of solids and semi-solids. In this way, this deformation science is used to measure fluid properties, understand structure-deformation relations, modelling flow behavior, and simulate deformation behavior under processing conditions (AMORIM et al., 2021; GEISSBERGER et al., 2017; LIU et al., 2020; NELSON; EWOLDT, 2017). Moreover, rheology can be associated with several physical variables and mechanical properties such as viscosity, elasticity, and granular flow, which can be measured by different equipment and analytical techniques.

Rheometry refers to the experimental technique in which a rheometer is used to determine rheological properties (GRIZZUTI, 2014). Numerous rheometric tests can be performed to assess the flow and deformation properties of simple and complex materials (JÓŹWIAK; BONCEL, 2020). In this analytical technique, the material is positioned in an apparatus called geometry, which moves according to the selected technology (rotation or oscillation) (MEZGER, 2014). Figure 1.1 illustrates some geometry models and their application to different types of materials.
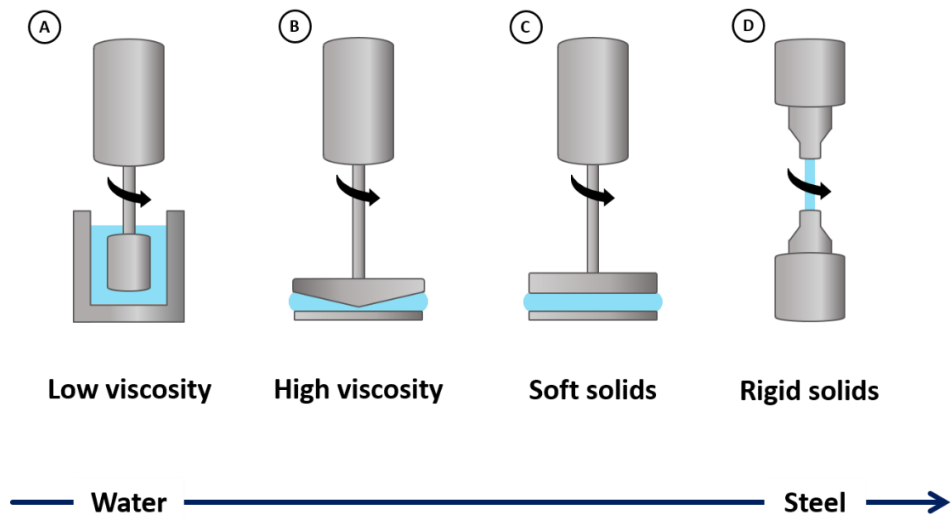
Figure 1.1 Different models of rheometric geometries for applications in materials of varied structure, ranging from water to steel; (A) concentric cylinders, (B) cone and plate, (C) parallel plate, and (D) cylindrical torsion.

1.2 Rotational and oscillatory rheology

Rheology can be classified according to its capacity and form of characterization, being divided into rotational rheology, known for measuring viscosity and steady properties, and oscillatory rheology, known for measuring viscoelastic compounds and dynamic properties (HUANG et al., 2016; KITAYAMA; YANG, 2021; NAJI-TABASI; RAZAVI, 2017; RAZI et al., 2020). Both procedures use two plates model to perform the analyzes. In this model, the sample is positioned between two plates, in which one is static and the other moves in different ways (geometry), then, the type of movement of the geometry is decisive to determine which rheological variable will be identified by the detector (LONG et al., 2015) (Figure 1.2).

Rotational rheology is marked by the 360° rotation of the geometry during the test. A rotational analysis depends on shear stress (τ) and shear rate ($\dot{\gamma}$) (VADODARIA; ONYIANTA; SUN, 2018). The shear stress is influenced by the force (F) applied to the material as a function of the area (A). In the case of rheometry, the geometry area is used (Figure 1.2A). Meanwhile, the shear rate is influenced by the gap (h) between the plates and by the speed (v) at which it moves (Figure 1.2A) (LIANG et al., 2015).

According to Newton's law for viscosity, the ratio between shear stress and shear rate results in viscosity (η) (GONÇALVES et al., 2017; HARDY, 2018; JIANG et al.,

2019) (Figure 1.2A). In practice, a certain rotation speed is set and to fulfill this requirement, the geometry needs to perform a specific torque (force), which will depend on the material viscosity (CARDOSO et al., 2014). By this means, the Newton equation is applied and it is possible to obtain viscosity data. Thus, rotational rheology is a more sophisticated alternative to the viscosimeter, since more sensitive variables are applied to assess viscosity.

A Rotational measurements

$$\tau = F / A \qquad \dot{\gamma} = v / h$$

$$\eta = \tau / \dot{\gamma}$$

B Oscillatory measurements

$$\tau = F / A \qquad \gamma = S / h$$

$$G^* = \tau / \gamma$$

F - force   A - area   v - velocity   h - gap   S – deflection τ - shear stress

$\dot{\gamma}$ - shear rate γ - strain η - viscosity G^* - complex modulus
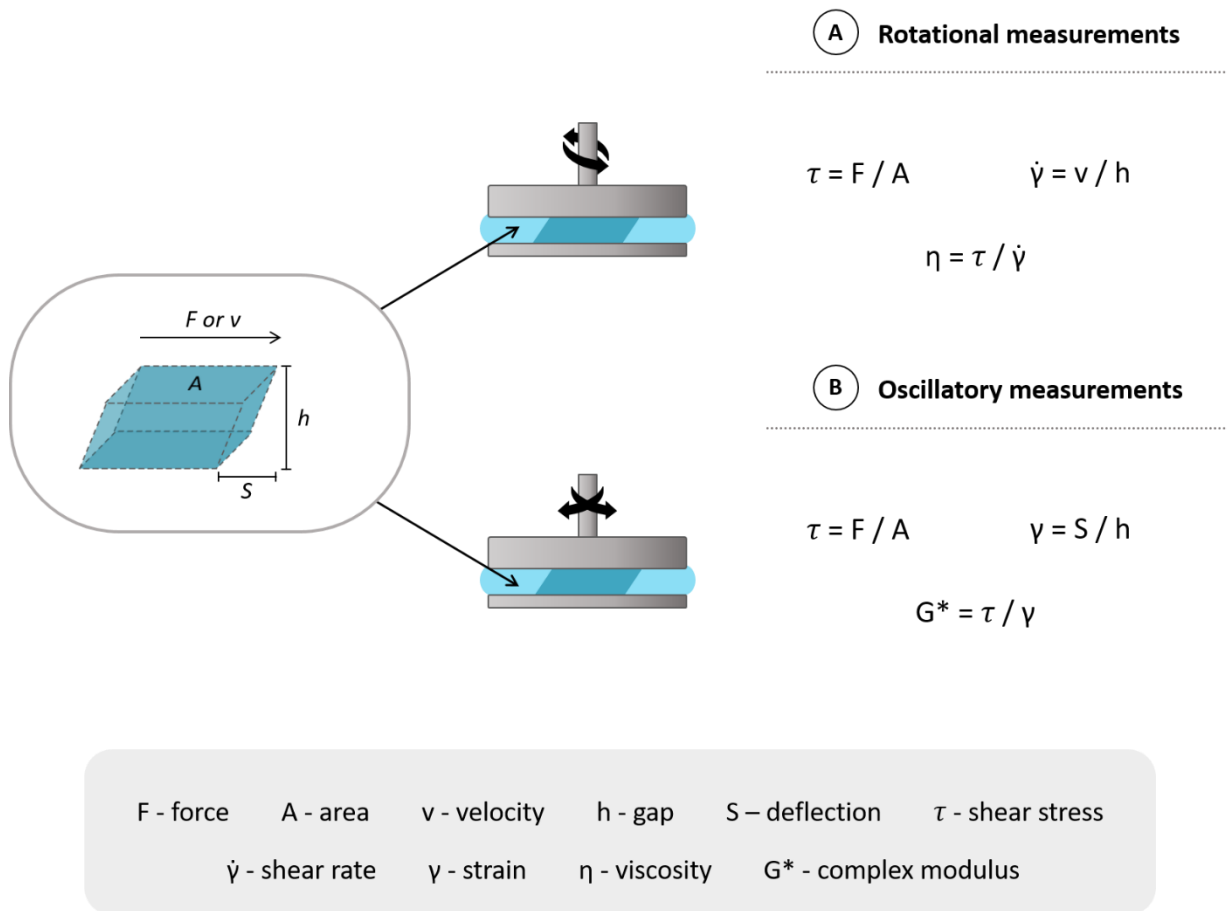
Figure 1.2 Representation of material's deformation inside the geometry, in conjunction with the variables and equations used to determine (A) viscosity, in a rotational test, and (B) complex modulus, in an oscillatory test.

Oscillatory rheology uses 180º movements in both directions, moving to the right and then to the left (AMARATUNGA; RABENJAFIMANANTSOA; TIME, 2021). This pulsing movement provides the identification of a new variable, the deflection path (S), which is mathematically converted into the rheological measure responsible for characterizing the deformation of a material: the strain (γ) (Figure 1.2B) (SAFAEI; CASTORENA, 2020). From the observed strain, it is possible to quantify the complex

modulus (G*), which is the rheological response for identifying a viscoelastic material, also known as a complex material, which will be explained in more detail in section 1.3.

In summary, rotational rheology identifies the flow of a material when a force is applied, characterizing its viscosity. On the other hand, oscillatory rheology can determine the deformation of a compound characterizing its viscoelastic properties.

1.3 Viscoelasticity

The deformation behavior of a material under stress depends on how the molecules respond to an external energy, which can be thermal, mechanical, gravitational, or shear (BAHMANPOUR et al., 2011; MIESZALA et al., 2017; YUAN; CHUA; ZHOU, 2019). Thus, to stress a material, first an energy source is applied, then this stress is absorbed by the molecules, and finally the material can respond in two ways, releasing the applied energy or storing it (GLEZER; SUNDEEV, 2015; SHIN; RICHTER; GIANOLA, 2020).

This different behavior depends on the inter and intramolecular interactions of the components (SHIN; RICHTER; GIANOLA, 2020). Molecules with high mobility cannot storge energy, while molecules with dense structures can do it easily; these two characteristics are classified in rheology as viscous and elastic behavior, respectively (Aho et al., 2015). Hence, materials that respond releasing energy are known as liquid materials, presenting a viscous behavior. On the other hand, materials that respond storing energy are known as solid materials, showing elastic behavior.

In this sense, some components can respond exclusively in a viscous way (pure liquids or Newtonian fluids), exclusively in an elastic way (pure solids or Hookean solids), or present both responses to the same source of stress (complex or viscoelastic compounds). Most materials belong to the viscoelastic class (Figure 1.3) (PHAN-THIEN; MAI-DUY, 2017).

It is possible to identify these different deformation characteristics individually with the aid of oscillatory rheology, since, through strain values the G* modulus is calculated. Due to this fact, for the deformation represented by energy storage, there is the elastic modulus, also called the storage modulus (G'), while for the deformation represented by energy release, there is the viscous modulus, also called the loss modulus (G") (DUTY et al., 2018; SEOANE-VIAÑO et al., 2021).

VISCOUS　　　　　　　　**VISCOELASTIC**　　　　　　　　**ELASTIC**

Figure 1.3 Representation of the material's classification according to its deformation response, viscous, elastic or viscoelastic.

As mentioned before, an oscillatory rheometer uses two variables, strain (γ) and stress (τ), sinusoidally (in a continuous wave). The lag between the peak of each wave is called the phase angle delta (δ) (HENRIQUES et al., 2018; MODLER; MOHAMAD; LUBECK, 2021) (Figure 1.4). This angle always ranges between 0° and 90° (MARQUEZ et al., 2018).

For a completely rigid sample with ideally elastic behavior, such as metal or steel, there is no lag between γ and τ response curves, the opposite is observed for perfect fluids. Therefore, $\delta = 0°$ stands for ideally elastic deformation (Figure 1.5A) and $\delta = 90°$ for ideally viscous flow behavior (Figure 1.5B). All viscoelastic responses take place between these two extremes (Figure 1.5C) (ZAMORA et al., 2018).
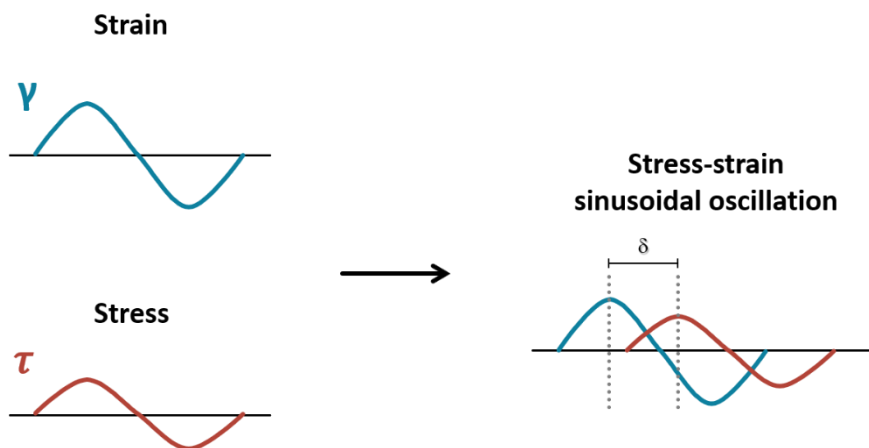
Figure 1.4 Hypothetical sinusoidal curve representing the oscillation of strain (γ) and shear stress (τ) during an oscillatory rheological analysis to identify the phase angle (δ).
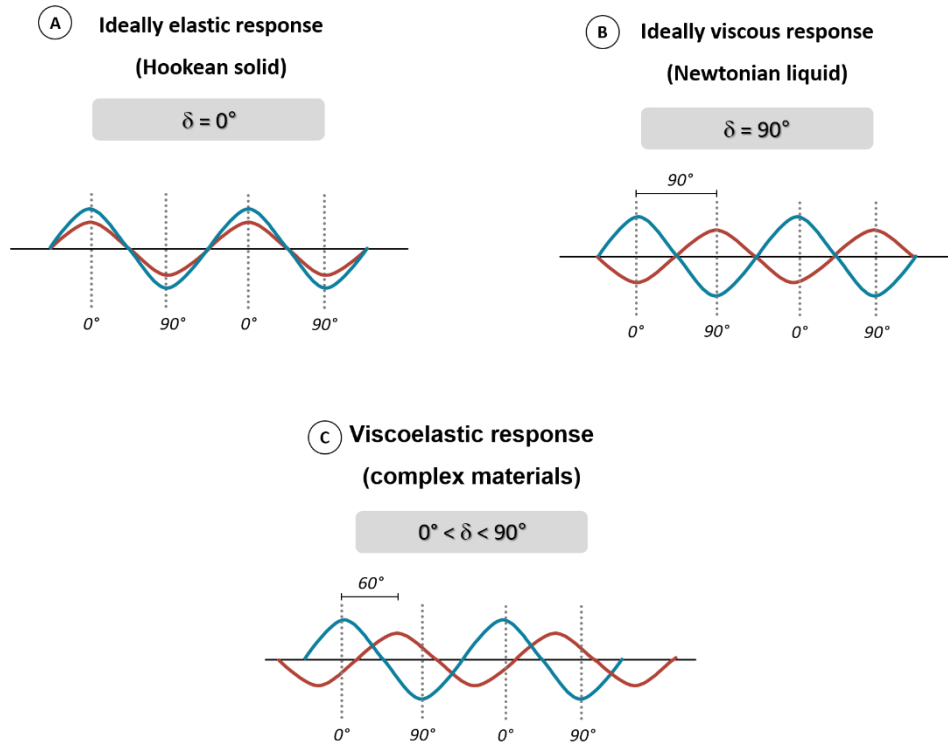
Figure 1.5 Hypothetical sinusoidal curve with representation of the phase angle (δ) for the deformation of a material (A) purely elastic (B) purely viscous and (C) viscoelastic.

Based on this, the angle δ is plotted below the G* vector, the part of the response that extends through the x axis is the value of the elastic deformation, while the part that extends through the y axis is the value of the viscous deformation, i.e., G' and G'' respectively (Figure 1.6) (LAI et al., 2021). Moreover, G* is also used to calculate the complex viscosity (η*) (Equation 1) (RABBANI; SCHMITT, 2018; ZARE; RHEE, 2019), which is a viscosity data that considers the complete viscoelastic deformation of materials and not just their flow behavior.

$$\eta^* = G^*/\omega \qquad (1)$$

From the Pythagorean triangle inferred in Figure 1.6, it is possible to calculate tangent of δ (tan δ) (Equation 2) (PINHO et al., 2021). Tan δ can be an important measurement for solid materials, since it provides information where viscous deformation has a strong influence on the material's behavior, even if the material still behaves as a solid compound (BOCHMANN et al., 2017).

$$\text{Tan } (\delta) = G''/G' \qquad (2)$$
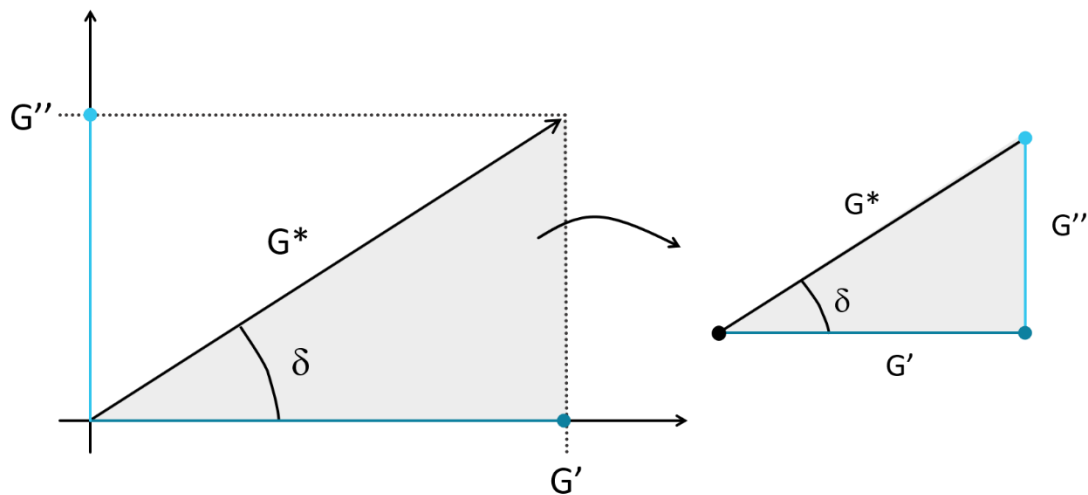
Figure 1.6 Vector diagram illustrating the relationship between complex modulus (G*) and the phase angle (δ), providing the quantification of storage modulus (G') and loss modulus (G").

Therefore, a rheometer operating in sinusoidal oscillation can easily separate the viscous and elastic portions of a material, enabling the identification of numerous types of deformations capable of influencing, individually, in its processing and molecular interaction with different components. For this reason, oscillatory shear rheology is the most recommended technique for developing pharmaceutical systems, especially those produced under stress conditions, such as high temperatures and mechanical forces.

1.4 References

AMARATUNGA, M.; RABENJAFIMANANTSOA, H. A.; TIME, R. W. Influence of low-frequency oscillatory motion on particle settling in Newtonian and shear-thinning non-Newtonian fluids. **Journal of Petroleum Science and Engineering**, v. 196, p. 107786, 2021.

AMORIM, P. A.; D'ÁVILA, M. A.; ANAND, R.; MOLDENAERS, P.; VAN PUYVELDE, P.; BLOEMEN, V. Insights on shear rheology of inks for extrusion-based 3D bioprinting. **Bioprinting**, v. 22, p. e00129, 2021.

BAHMANPOUR, H.; KAUFFMANN, A.; KHOSHKHOO, M. S.; YOUSSEF, K. M.; MULA, S.; FREUDENBERGER, J.; ECKERT, J.; SCATTERGOOD, R. O.; KOCH, C. C. Effect of stacking fault energy on deformation behavior of cryo-rolled copper and copper alloys. **Materials Science and Engineering A**, v. 529, n. 1, p. 230–236, 2011.

BOCHMANN, E. S.; ÜSTÜNER, E. E.; GRYCZKE, A.; WAGNER, K. G. Predicting melt rheology for hot-melt extrusion by means of a simple Tg-measurement. **European Journal of Pharmaceutics and Biopharmaceutics**, v. 119, p. 47–55, 2017.

CARDOSO, F. A.; JOHN, V. M.; PILEGGI, R. G.; BANFILL, P. F. G. Characterisation of rendering mortars by squeeze-flow and rotational rheometry. **Cement and Concrete Research**, v. 57, p. 79–87, 2014.

DUTY, C. et al. What makes a material printable? A viscoelastic model for extrusion-based 3D printing of polymers. **Journal of Manufacturing Processes**, v. 35, p. 526–537, 2018.

GEISSBERGER, R.; MALDONADO, J.; BAHAMONDE, N.; KELLER, A.; DRANSFELD, C.; MASANIA, K. Rheological modelling of thermoset composite processing. **Composites Part B: Engineering**, v. 124, p. 182–189, 2017.

GLEZER, A. M.; SUNDEEV, R. V. General view of severe plastic deformation in solid state. **Materials Letters**, v. 139, p. 455–457, 2015.

GONÇALVES, B. J.; PEREIRA, C. G.; LAGO, A. M. T.; GONÇALVES, C. S.; GIAROLA, T. M. O.; ABREU, L. R.; RESENDE, J. V. Thermal conductivity as influenced by the temperature and apparent viscosity of dairy products. **Journal of Dairy Science**, v. 100, n. 5, p. 3513–3525, 2017.

GRIZZUTI, N. Rheometry. Reference Module in Chemistry, **Molecular Sciences and Chemical Engineering**, p. 1–15, 2014.

GUZMÁN, E.; TAJUELO, J.; PASTOR, J. M.; RUBIO, M. A.; ORTEGA, F.; RUBIO, R. G. Shear rheology of fluid interfaces: Closing the gap between macro- and micro-rheology. **Current Opinion in Colloid and Interface Science**, v. 37, p. 33-48, 2018.

HARDY, Stuart. Coupling a frictional-cohesive cover and a viscous substrate in a discrete element model: First results of application to thick- and thin-skinned extensional tectonics. **Marine and Petroleum Geology**, v. 97, p. 32–44, 2018.

HENRIQUES, I. R.; BORGES, L. A.; COSTA, M. F.; SOARES, B. G.; CASTELLO, D. A. Comparisons of complex modulus provided by different DMA. **Polymer Testing**, v. 72, p. 394–406, 2018.

HUANG, J.; ZENG, S.; XIONG, S.; HUANG, Q. Steady, dynamic, and creep-recovery rheological properties of myofibrillar protein from grass carp muscle. **Food Hydrocolloids**, v. 61, p. 48–56, 2016.

JIANG, X.; LI, P.; DING, Z.; YANG, L.; ZHAO, J. Investigations on viscosity and flow behavior of polyphosphoric acid (PPA) modified asphalt at high temperatures. **Construction and Building Materials**, v. 228, p. 116610, 2019.

JÓŹWIAK, B.; BONCEL, S. Rheology of ionanofluids – A review. **Journal of Molecular Liquids**, 302, p. 112568, 2020.

KITAYAMA, S.; YANG, C. Steady-state dynamic response analysis of self-centering structural systems with viscous damping. **Soil Dynamics and Earthquake Engineering**, v. 150, p. 106926, 2021.

LAI, C. Q.; MARKANDAN, K.; LUO, B.; LAM, Y. C.; CHUNG, W. C.; CHIDAMBARAM, A. Viscoelastic and high strain rate response of anisotropic graphene-polymer nanocomposites fabricated with stereolithographic 3D printing. **Additive Manufacturing**, v. 37, p. 101721, 2021.

LIANG, J. Z.; CHEN, C. Y.; ZOU, S. Y.; TSUI, C. P.; TANG, C. Y.; ZHANG, S. D. Melt flow behavior of polypropylene composites filled with multi-walled carbon nanotubes during extrusion. **Polymer Testing**, v. 45, p. 41–46, 2015.

LIU, Z.; SONG, Y.; LIU, W.; LIU, R.; LANG, C.; LI, Y. Rheology of methane hydrate slurries formed from water-in-oil emulsion with different surfactants concentrations. **Fuel,** v. 275, p. 117961, 2020.

LONG, R.; MAYUMI, K.; CRETON, C.; NARITA, T.; HUI, C-Y. Rheology of a dual crosslink self-healing gel: Theory and measurement using parallel-plate torsional rheometry. **Journal of Rheology**, v. 59, n. 3, p. 643–665, 2015.

MARQUEZ, R.; FORGIARINI, A. M.; FERNÁNDEZ, J.; LANGEVIN, D.; SALAGER, J. L. New Interfacial Rheology Characteristics Measured using a Spinning-Drop Rheometer at the Optimum Formulation of a Simple Surfactant–Oil–Water System. **Journal of Surfactants and Detergents**, v. 21, n. 5, p. 611–623, 2018.

MEZGER, T. G. The Rheology Handbook: For users of rotational and oscillatory rheometers. Vincentz Network, Fourth Edition, 2020.

MIESZALA, M. et al. Micromechanics of Amorphous Metal/Polymer Hybrid Structures with 3D Cellular Architectures: Size Effects, Buckling Behavior, and Energy Absorption **Capability. Small**, v. 13, n. 8, 2017.

MODLER, L. E. A.; MOHAMAD, G.; LUBECK, A.; Hardening process of polymeric adhesive mortars: Approach by phase angle analysis from oscillatory rheometry. **Construction and Building Materials**, v. 271, p. 121521, 2021.

NAJI-TABASI, S.; RAZAVI, S. M. A. New studies on basil (Ocimum bacilicum L.) seed gum: Part III – Steady and dynamic shear rheology. **Food Hydrocolloids**, v. 67, p. 243–250, 2017.

NELSON, A. Z.; EWOLDT, R. H. Design of yield-stress fluids: A rheology-to-structure inverse problem. **Soft Matter**, v. 13, n. 41, p. 7578–7594, 2017.

PHAN-THIEN, N.; MAI-DUY, N. Understanding Viscoelasticity: an introduction to rheology, Springer, Third Edition, 2017.

PINHO, L. A. G.; LIMA, A. L.; SA-BARRETO, L. L.; GRATIERI, T.; GELFUSO, G.; MARRETO, R. N.; CUNHA-FILHO, Marcilio. Preformulation studies to guide the

production of medicines by fused deposition modeling 3D printing. **AAPS PharmSciTech**, 2021.

RABBANI, A.; SCHMITT, Do. R. Ultrasonic shear wave reflectometry applied to the determination of the shear moduli and viscosity of a viscoelastic bitumen. **Fuel**, v. 232, p. 506–518, 2018.

RAZI, S. M.; MOTAMEDZADEGAN, A.; SHAHIDI, S. A.; RASHIDINEJAD, A. Steady and dynamic shear rheology as a tool for evaluation of the interactions between egg white albumin and basil seed gum. **Rheologica Acta**, v. 59, n. 5, p. 317–331, 2020.

SAFAEI, F.; CASTORENA, C. Improved interpretation of asphalt binder parallel plate dynamic shear rheometer fatigue tests. **International Journal of Pavement Engineering**, v. 21, n. 1, p. 74–87, 2020.

SEOANE-VIAÑO, I.; JANUSKAITE, P.; ALVAREZ-LORENZO, C.; BASIT, A. W.; GOYANES, A. Semi-solid extrusion 3D printing in drug delivery and biomedicine: Personalised solutions for healthcare challenges. **Journal of Controlled Release** v. 332, p.367 -389 2021.

SHIN, J.; RICHTER, G.; GIANOLA, D. S. Suppressing instabilities in defect-scarce nanowires by controlling the energy release rate during incipient plasticity. **Materials and Design**, v. 189, 2020.
.
VADODARIA, S. S.; ONYIANTA, A J.; SUN, D. High-shear rate rheometry of micro-nanofibrillated cellulose (CMF/CNF) suspensions using rotational rheometer. **Cellulose**, v. 25, n. 10, p. 5535–5552, 2018.

YUAN, S.; CHUA, C. K.; ZHOU, K. 3D-Printed Mechanical Metamaterials with High Energy Absorption. **Advanced Materials Technologies**, v. 4, n. 3, 2019.

ZAMORA, J. M.; MARQUEZ, R.; FORGIARINI, A. M.; LANGEVIN, D.; SALAGER, Jean Louis. Interfacial rheology of low interfacial tension systems using a new oscillating spinning drop method. **Journal of Colloid and Interface Science**, v. 519, p. 27–37, 2018.

ZARE, Yasser; RHEE, Kyong Yop. Modeling of viscosity and complex modulus for poly (lactic acid)/poly (ethylene oxide)/carbon nanotubes nanocomposites assuming yield stress and network breaking time. **Composites Part B: Engineering**, v. 156, p. 100–107, 2019.

CHAPTER 2 - RHEOLOGICAL APPLICATIONS FOR PHARMACEUTICAL SOLID MATERIALS AND PROCESSING TECHNIQUES USED TO DEVELOP PHARMACEUTICAL SYSTEMS

This part of the work describes the theoretical application of oscillatory rheology to analyze solid compounds, especially materials developed by hot-melt extrusion and fused deposition modeling 3D printing.

2.1 Small amplitude oscillatory shear (SAOS)

To properly evaluate the formulation's processability and characterize its components, it is necessary to ensure that the molecular structure will not be damaged or destroyed during the analysis. This chemical stability is difficult to be established with solid materials, since the extreme rigidity can make materials brittle, leading to fragile intramolecular bonding forces, which can break during oscillation tests and disable the evaluation, especially at temperatures in which the material still remains solid (LIU et al., 2019).

In this scenario, oscillatory shear tests can be divided into two regimes. The first one is the linear viscoelastic response (LVR) and the other is defined by a nonlinear measurement (BONILLA; ERTURK; KOKINI, 2020). The strain is the rheological variable that will control this phenomenon, as it represents the amplitude in which the deformation can occur. Thus, changes in the strain inside the LVR of the material do not modify the rheological response, whereas changes in the strain outside the LVR imply a non-constant deformation with risk of molecular destruction, making the analysis unfeasible (SONG et al., 2020).

The determination of the LVR is performed by an amplitude (strain) sweep test, in which the applied amplitude is increased from small to large at a fixed frequency, a transition between the linear and non-linear regimes appears (Figure 2.1) (GHORBANI et al., 2017). Therefore, the LVR is different for each material, being extensive for liquid compounds and short for solid compounds, making high strain values easily accepted by fluids, while the molecular control of elastic materials is more delicate (ELBADAWI et al., 2020; REDDY et al., 2017).

Methods that work with low strain values are known as SAOS (small amplitude oscillatory shear), while those that work with high strain values are known as LAOS (large amplitude oscillatory shear) (TOWNSEND; WILSON, 2018). As the LVR of solid materials is always formed by low strain values, the SAOS methodology must be chosen for the characterization of pharmaceutical systems developed by extrusion or 3D printing.
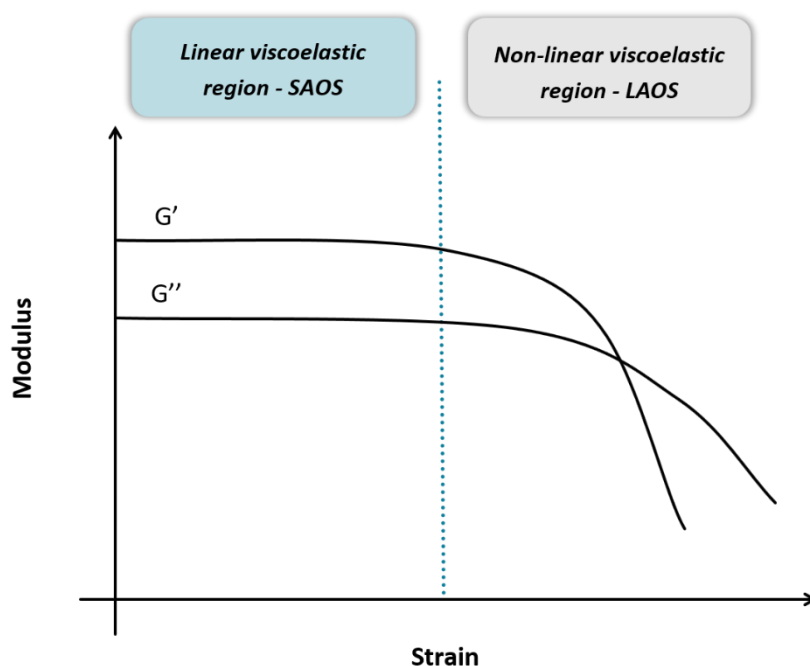
Figure 2.1 Hypothetical graphical representation of an amplitude sweep analysis in which the loss modulus (G') and storage modulus (G") are plotted. The green region indicates the linear viscoelastic response and the strain values that form the SAOS method. In contrast, the gray region indicates the non-linear viscoelastic response and the strain values that form the LAOS method.

2.2 Hot-melt extrusion and 3D printing

Polymers are one of the most complex viscoelastic materials, since these macromolecules can present different viscous and elastic behaviors simultaneously due to its high molecular weight, long chains, and varied inter and intra-molecular interactions (OSSWALD; RUDOLPH, 2013). Polymers are widely used in pharmaceuticals for the preparation of solid dispersions, in which, through a processing technique, the drug is dispersed or solubilized into the polymer matrix (PINHO et al., 2021; REPKA et al., 2018).

Hot-melt extrusion (HME) is a technique introduced to the pharmaceutical industry to elaborate these drug-loaded polymeric systems (SIMÕES; PINTO; SIMÕES, 2019). For this, polymer, drug, and excipients (if necessary) are introduced into the equipment where they reach the extruder screws and barrel, which are responsible for promoting a controlled shear rate and an increase in temperature, respectively (Figure 2.2) (BANDARI et al., 2021).
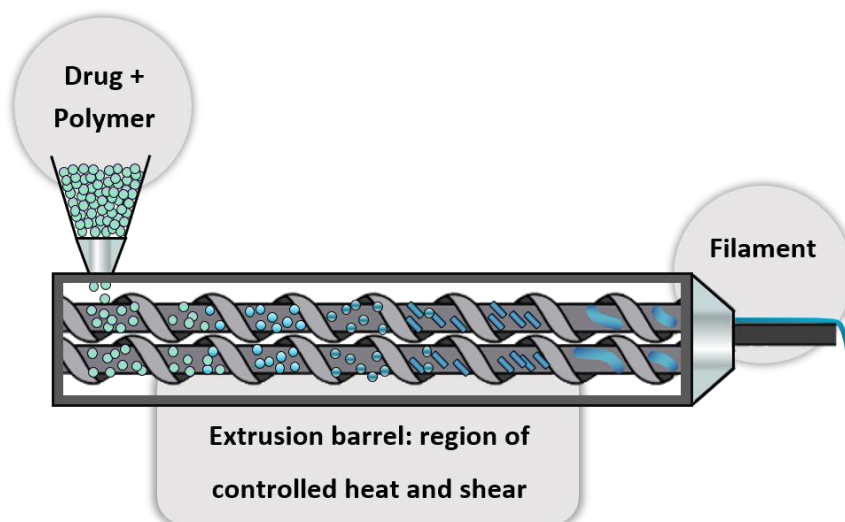
Figure 2.2. Illustration of the HME process indicating the feeding step, extrusion and development of the pharmaceutical filament.

In this way, the heat melts the material while the screws promote a homogeneous mixture of the formulation components. Additionally, the conjoint action of this thermal and mechanical stress provides strong polymer-drug molecular interactions, allowing the amorphization of the drug through its solubilization into the polymer matrix (NARALA et al., 2021). This non-crystalline profile is an important characteristic that significantly improves pharmaceutical performance. Finally, the molten material is eliminated from the extruder, gaining the shape of the selected die (outlet region of the equipment), which is generally cylindrical, forming pharmaceutical filaments (Figure 2.2) (TAMBE et al., 2021).

These drug-loaded filaments can be used to feed a fused deposition modeling 3D printing (FDM/3D) process (DUMPA et al., 2021). In this technology, the HME filament is pulled through two gears, which will guide the filament to the heater and the nozzle at high temperatures (Figure 2.3). As the filament reaches the final region of the 3D printer extruder, the material will melt, deforming with heat, and flowing through the nozzle,

which builds 3D structures layer-by-layer from the movement of the nozzle and/or the support table where the object is being built (BHAGIA et al., 2021).
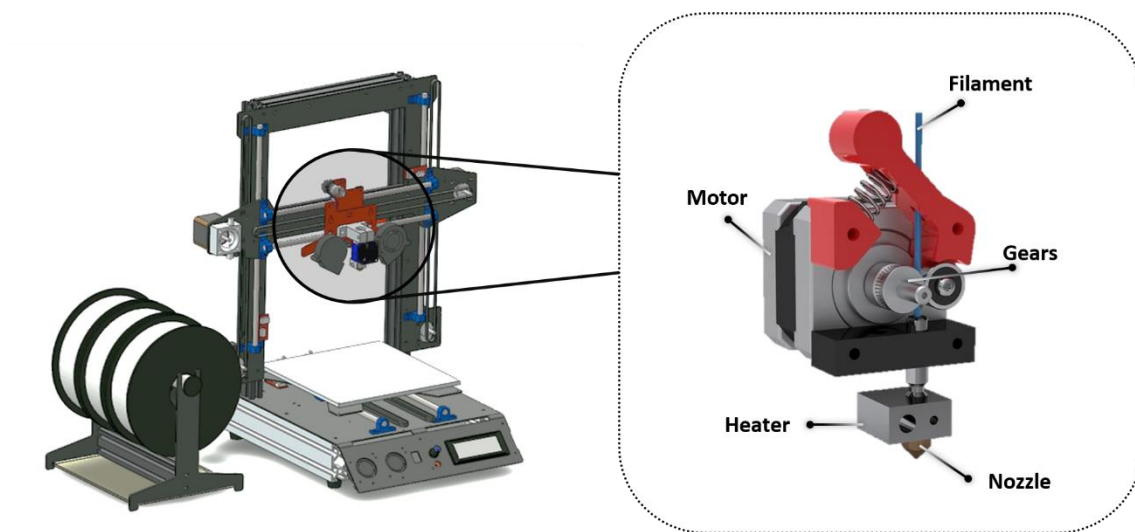
Figure 2.3. Illustration of an FDM 3D printer and indication of the different parts that form the 3D printer extruder (dotted square).

Based on these emerging technologies for processing pharmaceutical materials, it is possible to infer that the knowledge of polymer rheological deformation and viscoelastic behavior as a function of time, shear and temperature is of great assistance in tailoring the adequate process conditions and choosing suitable polymer carriers for extrusion, as well as predicting the processability and polymer-drug interaction.

For this scenario, complex oscillatory rheological tests and mathematical equations are needed to analyze polymeric materials and pharmaceutical extrudates. Commonly, rheological measurements of viscosity, modulus, and tangent of angle δ are evaluated as a function of frequency and temperature variations (AHO et al., 2015; ELBADAWI et al., 2020).

Within the limited number of works that apply oscillatory rheology to HME and FDM/3D, the frequency sweep test is the most performed (BOETKER et al., 2016; ILYÉS et al., 2019; ISREB et al., 2019). In this experimental technique, temperature and strain are constant and an increasing frequency is applied to the material in order to evaluate their moduli (G' and G'') and complex viscosity (Figure 2.4) (MARRETO et al., 2020; SOLANKI et al., 2019). This provides the time-dependent behavior of a sample, since low frequencies simulate slow motion or slow processing conditions (green region

Figure 2.4) and high frequencies simulate fast motion or fast processing conditions (grey region Figure 2.4) (AHO et al., 2016; AIREY et al., 2016).

When applying to HME and FDM/3D, frequency sweeps are proven methods to choose the proper screw rotation and the printing speed, as it can collect information on the behavior and inner structure of the formulation under procedure parameters (shear and temperature are constant) and assess the time required for the material to deform optimally (AHO et al., 2016; BERTOLINO et al., 2021). In most researches, several possible processing temperatures are selected and the frequency sweep analysis is performed in these different isotherms. Therefore, the condition that provides adequate deformation in short time and low temperature is considered ideal (BOCHMANN et al., 2017; MONSCHKE; KAYSER; WAGNER, 2020; SOLANKI; GUPTA; SERAJUDDIN, 2018)
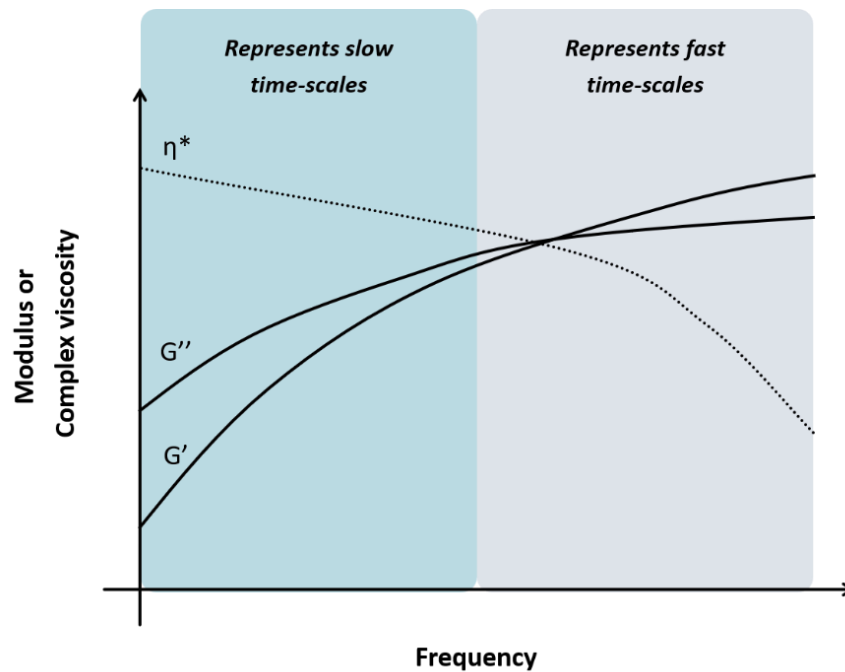
Figure 2.4. Hypothetical graphical representation of a frequency sweep analysis in which the loss modulus (G'), storage modulus (G") and complex viscosity (η^*) are plotted. The green region indicates the low frequency values, used to represent slow processing conditions, while the gray region indicates the high frequency values, used to represent fast processing conditions.

Rheological temperature ramp analysis is a widely explored test in materials science for evaluating polymers suitable to extrusion and 3D printing (CHEN et al., 2020; LAI et al., 2021). In this scenario, this oscillatory assay has been increasingly inserted in

the characterization step of pharmaceutical mixtures and filaments produced for HME or FDM/3D (AHO et al., 2017; ELBADAWI et al., 2020). In this experiment, rheological patterns are monitored with temperature variation (Figure 2.5).

In practice, the viscoelastic behavior of the material is evaluated as a function of temperature, in order to assess its deformation capacity at different heat profiles, to enable the ideal definition of thermal and stress for extrusion or printing process (AZAD et al., 2020). For pharmaceutical systems developed by HME and FDM/3D, the elastic deformation (marked by G') cannot be too high, otherwise the polymer will not deform, consequently the polymer-drug interaction is impaired. However, if the viscous behavior (marked by G") is greater, the deformation will be so intense that the polymer will not recover and solidify after extrusion or printing (AHO et al., 2015).
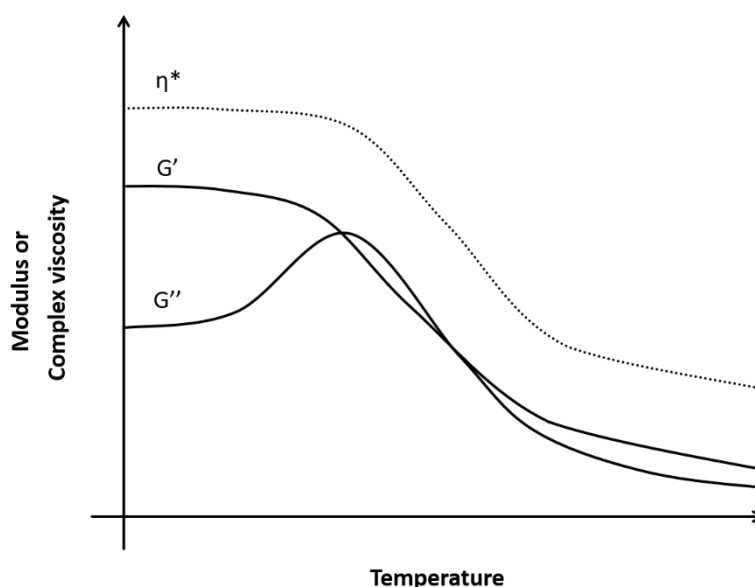

Figure 2.5. Hypothetical graphical representation of a temperature ramp analysis in which the loss modulus (G'), storage modulus (G") and complex viscosity (η^*) are plotted.

Moreover, for assessing the complete deformation of the formulation, complex viscosity and complex modulus are monitored as they gather information about the resistance of flow and deformation, respectively, considering the viscoelasticity of the material (PINHO et al., 2021). Additionally, for characterization purposes, this analysis is commonly performed to assess the glass transition region (Tg) and melting point (Tm) of the polymer (CUCALON et al., 2019; SADEGHI-MEHR et al., 2018).

For a solid polymer, the glass transition range starts at the first signs of materials softening and it ends when the molten state has been completely reached (green line

Figure 2.6) (BARBA; ARIAS; GARCIA-GONZALEZ, 2020). In this way, the Tg temperature is established approximately in the middle of the Tg range and it can change according to the proposed mathematical method of interpretation: temperature onset of G' decay (YONG et al., 2017), peak preceding G" decay (XIE et al., 2020) or peak of tan δ (LIPIŃSKA; IMIELA, 2019). Since tan δ considers both viscous and elastic deformation it is the most described method for calculating Tg temperature.
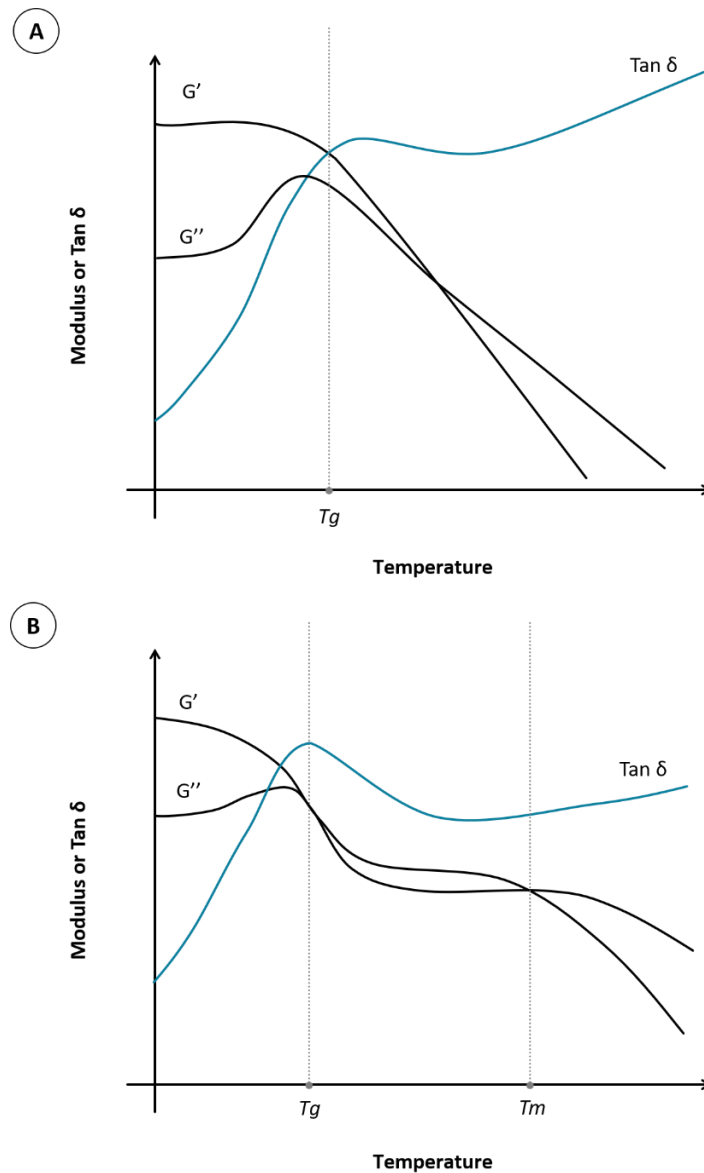
Figure 2.6. Hypothetical graphical representation of a temperature ramp analysis in which the loss modulus (G'), storage modulus (G") and tangent of the angle (Tan δ) are plotted. Tan δ peak indicates the glass transition temperature (Tg) of (A) an amorphous polymer and (B) a crystalline polymer, in which the melting point (Tm) is also represented and indicated by the modulus crossover.

The melting point, in a rheological temperature ramp analysis is classified as the crossover temperature (G' = G'') (CUCALON et al., 2019). Figure 2.6A shows the viscoelastic profile of an amorphous polymer, indicating its Tg temperature, while figure 2.6B shows the viscoelastic profile of a crystalline polymer, showing Tg and Tm.

Conclusively, besides supporting the identification of the best process conditions, a temperature ramp analysis is also capable of evaluating crystalline profile, decomposition, compatibility and capacity for molecular interaction (PINHO et al., 2021; SAMARO et al., 2020). Moreover, the intrinsic characterization proposed by this rheological test can provide information during and after the material is stressed, since the rheometer is able to return to ambient conditions while continues to monitor the rheological variables.

In this way, this analytical tool can identify the influence of processing conditions on product stability, predicting possible degradation, incompatibility and crystallization caused by extrusion or printing. Hence, oscillatory rheology is a perfect instrument for guaranteeing 3D drug products with pharmaceutical requirements maintained.

2.3 References

AHO, J.; VAN RENTERGHEM, J.; ARNFAST, L.; DE BEER, T.; RANTANEN, J. The flow properties and presence of crystals in drug-polymer mixtures: Rheological investigation combined with light microscopy. **International Journal of Pharmaceutics**, v. 528, n. 1–2, p. 383–394, 2017

AHO, J.; BOETKER, J. P.; BALDURSDOTTIR, S.; RANTANEN, J. Rheology as a tool for evaluation of melt processability of innovative dosage forms. **International Journal of Pharmaceutics**, v. 494, n. 2, p. 623-642, 2015.

AHO, J.; EDINGER, M.; BOTKER, J.; BALDURSDOTTIR, S.; RANTANEN, J. Oscillatory Shear Rheology in Examining the Drug-Polymer Interactions Relevant in Hot Melt Extrusion. **Journal of Pharmaceutical Sciences**, v. 105, n. 1, p. 160–167, 2016.

AIREY, G. D.; GRENFELL, J. R. A.; APEAGYEI, A.; SUBHY, A.; LO PRESTI, D. Time dependent viscoelastic rheological response of pure, modified and synthetic bituminous binders. **Mechanics of Time-Dependent Materials**, v. 20, n. 3, p. 455–480, 2016.

AZAD, M. A.; OLAWUNI, D.; KIMBELL, G.; BADRUDDOZA, A. Z.; HOSSAIN, S.t; SULTANA, T. Polymers for extrusion-based 3D printing of pharmaceuticals: A holistic materials–process perspective. **Pharmaceutics**, v.12, n. 2, p. 124, 2020.

BANDARI, S.; NYAVANANDI, D.; DUMPA, N.; REPKA, M. A. Coupling hot melt extrusion and fused deposition modeling: Critical properties for successful performance. **Advanced Drug Delivery Reviews**, v. 172, p. 52-63, 2021.

BARBA, D.; ARIAS, A.; GARCIA-GONZALEZ, D. Temperature and strain rate dependences on hardening and softening behaviours in semi-crystalline polymers: Application to PEEK. **International Journal of Solids and Structures**, v. 182–183, p. 205–217, 2020.

BERTOLINO, M.; BATTEGAZZORE, D.; ARRIGO, R.; FRACHE, A. Designing 3D printable polypropylene: Material and process optimisation through rheology. **Additive Manufacturing**, v. 40, p. 101944, 2021.

BHAGIA, S. et al. Critical review of FDM 3D printing of PLA biocomposites filled with biomass resources, characterization, biodegradability, upcycling and opportunities for biorefineries. **Applied Materials Today**, v.24, p. 101078, 2021.

BOCHMANN, E. S.; ÜSTÜNER, E. E.; GRYCZKE, A.; WAGNER, K. G. Predicting melt rheology for hot-melt extrusion by means of a simple Tg-measurement. **European Journal of Pharmaceutics and Biopharmaceutics**, v. 119, p. 47–55, 2017.
BOETKER, J.; WATER, J. J.; AHO, J.; ARNFAST, L.; BOHR, A.; RANTANEN, J. Modifying release characteristics from 3D printed drug-eluting products. **European Journal of Pharmaceutical Sciences**, v. 90, p. 47–52, 2016.

BONILLA, J. C.; ERTURK, M. Y.; KOKINI, J. L. Understanding the role of gluten subunits (LMW, HMW glutenins and gliadin) in the networking behavior of a weak soft wheat dough and a strong semolina wheat flour dough and the relationship with linear and non-linear rheology. **Food Hydrocolloids**, v. 108, p. 106002, 2020.

CHEN, Q.; HAN, Lu; REN, J.; RONG, L.; CAO, P.; ADVINCULA, Rigoberto C. 4D Printing via an Unconventional Fused Deposition Modeling Route to High-Performance Thermosets. **ACS Applied Materials and Interfaces**, v. 12, n. 44, p. 50052–50060, 2020.

CUCALON, L. G.; KASEER, F.; ARÁMBULA-MERCADO, E.; EPPS MARTIN, A.; MORIAN, N.; POURNOMAN, S.; HAJJ, E. The crossover temperature: significance and application towards engineering balanced recycled binder blends. **Road Materials and Pavement Design**, v. 20, n. 6, p. 1391–1412, 2019.

DUMPA, N.; BUTREDDY, A.; WANG, H.; KOMANDURI, N.; BANDARI, Suresh; REPKA, Michael A. 3D printing in personalized drug delivery: An overview of hot-melt extrusion-based fused deposition modeling. **International Journal of Pharmaceutics**, v.600, p. 120501, 2021.

ELBADAWI, M.; GUSTAFFSON, T.; GAISFORD, S.; BASIT, A. W. 3D printing tablets: Predicting printability and drug dissolution from rheological data. **International Journal of Pharmaceutics**, v. 590, p. 116898, 2020.

GHORBANI, M.; AI, J.; NOURANI, M. R.; AZAMI, M.; HASHEMI BENI, B.; ASADPOUR, S.; BORDBAR, S. Injectable natural polymer compound for tissue

engineering of intervertebral disc: In vitro study. **Materials Science and Engineering C**, v. 80, p. 502–508, 2017.

ILYÉS, K.; KOVÁCS, N. K.; BALOGH, A.; BORBÁS, E.; FARKAS, B.; CASIAN, T.; MAROSI, G.; TOMUȚĂ, I.; NAGY, Z. K. The applicability of pharmceutical polymeric blends for the fused deposition modelling (FDM) 3D technique: Material considerations–printability–process modulation, with consecutive effects on in vitro release, stability and degradation. **European Journal of Pharmaceutical Sciences**, v. 129, p. 110–123, 2019.

ISREB, A.; BAJ, K.; WOJSZ, M.; ISREB, M.; PEAK, M.; ALHNAN, M. A. 3D printed oral theophylline doses with innovative 'radiator-like' design: Impact of polyethylene oxide (PEO) molecular weight. **International Journal of Pharmaceutics**, v. 564, p. 98–105, 2019.

LAI, C. Q.; MARKANDAN, K.; LUO, B.; LAM, Y. C.; CHUNG, W. C.; CHIDAMBARAM, A. Viscoelastic and high strain rate response of anisotropic graphene-polymer nanocomposites fabricated with stereolithographic 3D printing. **Additive Manufacturing**, v. 37, p. 101721, 2021.

LIPIŃSKA, M.; IMIELA, M. Morphology, rheology and curing of (ethylene-propylene elastomer/hydrogenate acrylonitrile-butadiene rubber) blends reinforced by POSS and organoclay. **Polymer Testing**, v. 75, p. 26–37, 2019.

LIU, J.; ZHAO, Z.; WANG, W.; MAYS, J. W.; WANG, S. Q. Brittle-ductile transition in uniaxial compression of polymer glasses. **Journal of Polymer Science, Part B: Polymer Physics**, v. 57, n. 12, p. 758–770, 2019.

MARRETO, R. N.; CARDOSO, G.; DOS SANTOS SOUZA, B.; MARTIN-PASTOR, M.; CUNHA-FILHO, M.; TAVEIRA, S. F.; CONCHEIRO, A.; ALVAREZ-LORENZO, C. Hot melt-extrusion improves the properties of cyclodextrin-based poly(pseudo)rotaxanes for transdermal formulation. **International Journal of Pharmaceutics**, v. 586, p. 119510, 2020.

MONSCHKE, M.; KAYSER, K.; WAGNER, K. G. Processing of polyvinyl acetate phthalate in hot-melt extrusion-preparation of amorphous solid dispersions. **Pharmaceutics**, v. 12, n. 4, p. 337, 2020.

NARALA, S.; NYAVANANDI, D.; SRINIVASAN, P.; MANDATI, P.; BANDARI, S.; REPKA, M. A. Pharmaceutical Co-crystals, Salts, and Co-amorphous Systems: A novel opportunity of hot-melt extrusion. **Journal of Drug Delivery Science and Technology**, v.61, p. 102209, 2021.

OSSWALD, T. A.; RUDOLPH, N. S. Polymer rheology: fundamentals and applications. Carl Hanser, München, 2015.

PINHO, L. A. G.; LIMA, A. L.; SA-BARRETO, L. L.; GRATIERI, T.; GELFUSO, G.; MARRETO, R. N.; CUNHA-FILHO, M. Preformulation studies to guide the production of medicines by fused deposition modeling 3D printing. **AAPS PharmSciTech**, 2021.

REDDY, S. M. M.; DORISHETTY, P.; AUGUSTINE, G.; DESHPANDE, A. P.; AYYADURAI, N.; SHANMUGAM, G. A Low-Molecular-Weight Gelator Composed

of Pyrene and Fluorene Moieties for Effective Charge Transfer in Supramolecular Ambidextrous Gel. **Langmuir**, v. 33, n. 47, p. 13504–133514, 2017.

REPKA, M. A.; BANDARI, S.; KALLAKUNTA, V. R.; VO, A. Q.; MCFALL, H.; PIMPARADE, M. B.; BHAGURKAR, A. M. Melt extrusion with poorly soluble drugs – An integrated review. **International Journal of Pharmaceutics**, v. 535, n. 1–2, p. 68–85, 2018.

SADEGHI-MEHR, A.; RAUDSEPP, P.; BRÜGGEMANN, D. A.; LAUTENSCHLAEGER, R.; DRUSCH, S. Dynamic rheology, microstructure and texture properties of model porcine meat batter as affected by different cold-set binding systems. **Food Hydrocolloids**, v. 77, p. 937–944, 2018.

SAMARO, A.; JANSSENS, P.; VANHOORNE, V.; VAN RENTERGHEM, J.; EECKHOUT, M.; CARDON, L.; DE BEER, T.; VERVAET, C. Screening of pharmaceutical polymers for extrusion-Based Additive Manufacturing of patient-tailored tablets. **International Journal of Pharmaceutics**, v. 586, p. 119591, 2020.

SIMÕES, M. F.; PINTO, R. M. A.; SIMÕES, S. Hot-melt extrusion in the pharmaceutical industry: toward filing a new drug application. **Drug Discovery Today**, v. 24, n. 9, p. 1749-1768, 2019.

SOLANKI, N. G.; GUMASTE, S. G.; SHAH, A. V.; SERAJUDDIN, A. T. M. Effects of Surfactants on Itraconazole-Hydroxypropyl Methylcellulose Acetate Succinate Solid Dispersion Prepared by Hot Melt Extrusion. II: Rheological Analysis and Extrudability Testing. **Journal of Pharmaceutical Sciences**, v. 108, n. 9, p. 3063–3073, 2019.

SOLANKI, N.; GUPTA, S. S.; SERAJUDDIN, A. T. M. Rheological analysis of itraconazole-polymer mixtures to determine optimal melt extrusion temperature for development of amorphous solid dispersion. **European Journal of Pharmaceutical Sciences**, v. 111, p. 482–491, 2018.

SONG, H. Y.; FAUST, L.; SON, J.; KIM, M.; PARK, S. J.; AHN, S. K.; WILHELM, M.; HYUN, K. Small and medium amplitude oscillatory shear rheology of model branched polystyrene (PS) melts. **Polymers**, v. 12, n. 2, p. 365, 2020.

TAMBE, S.; JAIN, D.; AGARWAL, Y.; AMIN, P. Hot-melt extrusion: Highlighting recent advances in pharmaceutical applications**. Journal of Drug Delivery Science and Technology**, v. 63, p. 102452, 2021.

TOWNSEND, A. K.; WILSON, H. J. Small- and large-amplitude oscillatory rheometry with bead–spring dumbbells in Stokesian Dynamics to mimic viscoelasticity. **Journal of Non-Newtonian Fluid Mechanics**, v. 261, p. 136–152, 2018.

XIE, R. et al. Glass transition temperature from the chemical structure of conjugated polymers. **Nature Communications**, v. 11, n. 1, p. 893, 2020.

YONG, A. X. H.; SIMS, G. D.; GNANIAH, S. J. P.; OGIN, S. L.; SMITH, P. A. Heating rate effects on thermal analysis measurement of Tg in composite materials. **Advanced Manufacturing: Polymer and Composites Science**, v. 3, n. 2, p. 43–51, 2017.

CHAPTER 3 - OSCILLATORY SHEAR RHEOLOGY AS AN IN-PROCESS CONTROL TOOL FOR 3D PRINTING TABLETS PRODUCTION BY FUSED DEPOSITION MODELING

The objective of this part of the work was to apply oscillatory shear rheology as an in-process quality control tool to elaborate tablets by fused deposition modeling 3D printing, in order to obtain optimized processing conditions and stable pharmaceutical properties.

3.1 Introduction

In the current stage of 3D technology applied in the development of pharmaceuticals, a trial-and-error methodology still predominates, in which several materials are tested under numerous processing conditions with little capacity for anticipating the quality parameters of the printed medicines (CASTRO et al., 2021).
In this way, to assist printability requirements and successful feedability of extruded filaments, mechanical properties, such as stiffness, toughness, and ductility, have been evaluated in recent studies to determine formulations that would withstand the mechanical stress promoted by a FDM 3D printer (XU et al., 2020a; YANG et al., 2021). However, this characterization is not enough to select printable materials and properly define their printing parameters since thermal, rheological, and morphological variables contribute simultaneously to 3D printing (SAMARO et al., 2020; SEOANE-VIAÑO et al., 2021). Furthermore, molecular interactions between the formulation components can modify their deformation and consequently the printing step, making conventional mechanical evaluations useless (SILVA et al., 2021).

Conversely, oscillatory shear rheology is a technique that uses sinusoidal stress-strain to assess the deformation of viscoelastic materials, analyzing the temperature, shear, and time-dependent behavior of the viscous and elastic portion to describe their molecular conformation in different thermal-shear conditions, which makes this technique ideal for characterizing drug products developed by HME and FDM (AHO et al., 2015). In this sense, rheology has been increasingly explored in materials science to optimize printing processes and comprehend which properties make a material printable (BERTOLINO et al., 2021). Yet, there is still a lack of knowledge and applications of

such assays for pharmaceutical materials in additive manufacturing (SEOANE-VIAÑO et al., 2021).

In this sense, this work aimed to develop an in-process quality control protocol for HME filaments based on oscillatory shear rheology together with mechanical evaluations and thermal analysis to obtain a proper assessment of the filaments that can be used in a FDM 3D printer for pharmaceutical purposes. For this, hot-melt extruded filaments of polyvinyl alcohol (PVA) were produced as a matrix model containing different plasticizer ratios. Then, tablets were produced with these filaments and were evaluated based on pharmaceutical quality parameters.

3.2 Material and methods

3.2.1 Material

Parteck® MXP (PVA, polyvinyl alcohol, lot F1952064) was donated by Merck (Darmstadt, Germany), and glycerin (GLY, lot 58591) was purchased from Dinâmica (São Paulo, Brazil).

3.2.2 Preparation of filaments by hot-melt extrusion

Filaments were prepared by combining the polymer PVA with GLY, a plasticizer commonly used for this matrix (ARIANTO et al., 2021; CHEN et al., 2020; HOSSEINI; NABID, 2020). The mixtures of PVA-GLY were prepared by varying the plasticizer concentrations from 10 to 40 % w/w. First, the liquid plasticizer was incorporated into the polymer with a mortar and pestle. Then, to guarantee samples' homogenization, the components were mixed by a vertical M2 mixer (Powdermix, Santos, Brazil) for 5 min. Finally, PVA-GLY mixtures were extruded without recirculation in a co-rotating conical twin-screw extruder HME with a die diameter of 1.8 mm (HAAKE MiniCTW, ThermoScientific, Waltham, MA, USA) coupled to a filament tractor with air cooling system and an automated diameter measurement model FTR1 (Filmaq3D, Curitiba, Brazil). For each filament, 30 g of the polymer-plasticizer mixture were extruded, producing filaments with approximately 100 cm length.

The HME rotation was 50 rpm, and extrusion temperatures were set according to the formulation composition to obtain an adequate extrusion flow (Table 3.1). Moreover, the air cooling of the filament tractor was set at 1,000 rpm, and the traction speed was

adjusted according to HME powder feeding to produce a uniform filament diameter (PONSAR; WIEDEY; QUODBACH, 2020). All filaments were stored in a desiccator until characterization.

3.2.3 Filament diameter uniformity

Just after the samples reached room temperature, filaments diameters were measured with a digital caliper (Mitutoyo Sul Americana, São Paulo, Brazil). Thickness was measured at every 10 cm interval of the filament (GÜLTEKIN et al., 2021), totaling 10 measurements.

3.2.4 Mechanical properties

To evaluate the effect of the plasticizer ratio on the mechanical properties of the HME filaments, a tensile test was performed to identify their fracture force (n = 5). All analyses were executed in a universal testing machine (Shimadzu EZ test, Tokyo, Japan) equipped with a 5 kN load cell using wedge-type grips that move horizontally to tighten the grip on the filament (before analyzes) and vertically to perform the elongation test. The cell moved at a constant crosshead speed of 10 mm/min. The filament size was 60 mm, the gap between the cells was set at 30 mm, and the initial force was 1 N (HARYŃSKA et al., 2020).

Table 3.1 HME conditions, filament aspect obtained by optical microscopy (20×), water content obtained by TGA analysis, and FDM 3D printing temperature for each formulation.

Formulation	Extrusion conditions			Filament aspect	Water content (% w/w)	Printing temperature (^{o}C)
	Temperature (^{o}C)	Rotation (*rpm*)	Torque (*Nm*)			
PVA-GLY 10%	160	50	0.38		3.7	190
PVA-GLY 20%	150	50	0.34		5.2	180
PVA-GLY 30%	140	50	0.21		7.0	170
PVA-GLY 40%	130	50	0.23		7.7	160

3.2.5 Rheological analyses

The viscoelastic behavior of filaments was evaluated by a DHR-2 oscillatory rheometer (TA instruments, New Castle, DE, USA) equipped with a Peltier plate and a 40 mm parallel plate geometry, with a gap height fixed at 1 mm. Small amplitude oscillatory shear (SAOS) was determined to ensure tests were conducted in the linear viscoelastic range, which was defined by an amplitude oscillatory sweep test at a constant angular frequency (ω) of 6.28 rad/s and strain (γ) range from 0.001 to 1.000% (Figure 3.1). After this evaluation, a $\gamma = 0.002\%$ was chosen as the amplitude of deformation to perform the subsequent analyses since all samples showed a linear response in this strain value at the temperatures selected for the analyses (0 and 200 °C).

Temperature ramp analysis was performed from 200 to 0 °C at a heating rate of - 5 °C/min with $\omega = 6.28$ rad/s, to obtain the complex viscosity (η^*), glass transition (Tg), storage (G'), loss (G''), and complex (G^*) moduli. η^* and G^* was defined by (RABBANI; SCHMITT, 2018; ZARE; RHEE, 2019) and calculated as follow:

$$\eta^* = G^*/\omega \qquad\qquad (1)$$

$$G^* = \tau / \gamma \qquad\qquad (2)$$

were τ is the shear-stress amplitude.

Moreover, Tg was recognized by the inflection point of the angle δ tangent (tan δ) and was mathematically determined by the ratio between the loss and the storage moduli (PINHO et al., 2021; SADEGHI-MEHR et al., 2018):

$$Tan\ (\delta) = G''/G' \qquad\qquad (3)$$

Tan (δ) signal peak in a temperature ramp corresponds to the heat region where the material has the most viscous response to shear deformation but can still behave strongly as an elastic material, i.e., a solid compound with a liquid-like behavior. Therefore, in polymeric evaluations, tan δ peak is classified as the Tg temperature (DKIER et al., 2019).

All rheological analyses were conducted with the filaments placed on the geometry plate and softened for 2 min at 25 °C with a 1.2 mm gap. Then, to ensure that the filament would occupy the entire geometry plate, the samples were equilibrated at 110 °C in the measuring analysis gap (1 mm) for 2 min. Finally, the temperature was set to the starting temperature of the analysis, i.e., 0 or 200 °C, for amplitude oscillatory sweep tests; and 200 °C, for temperature ramp assays.
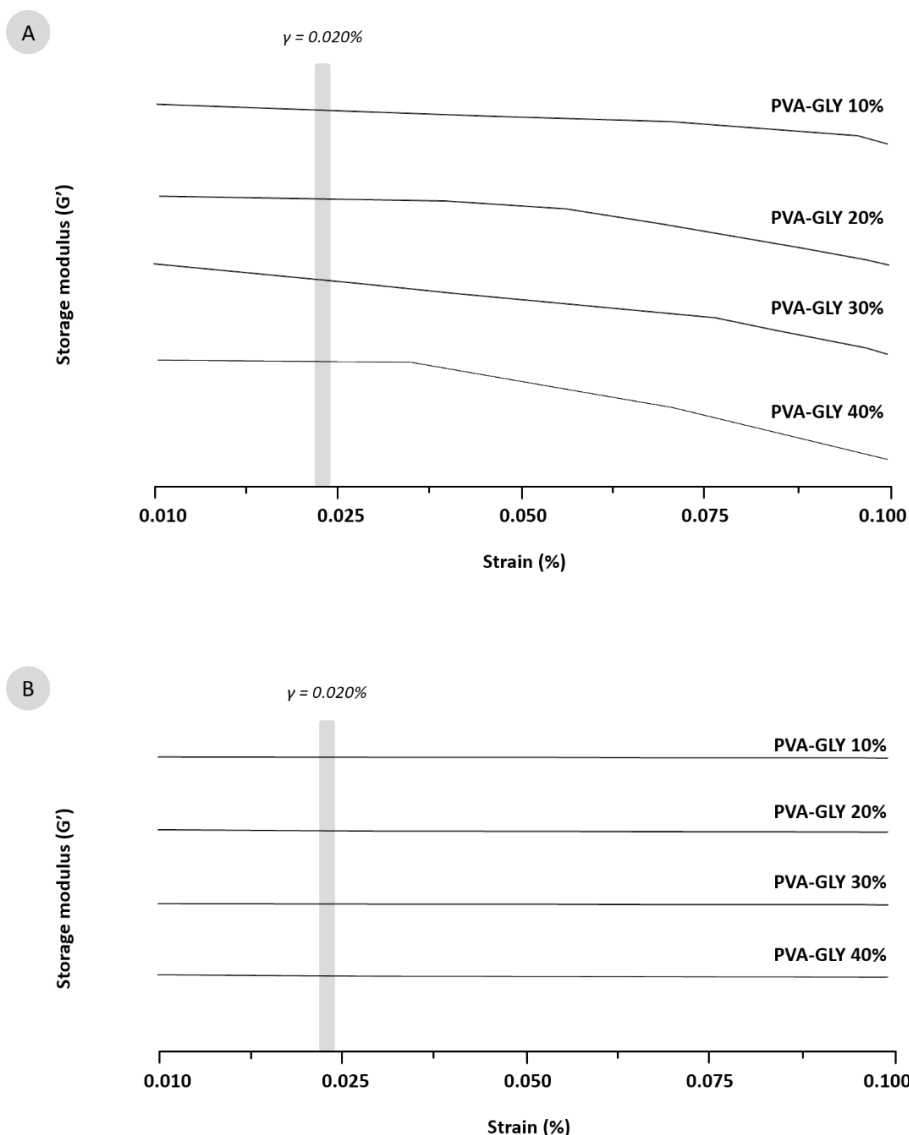
Figure 3.1 Amplitude sweep of PVA-GLY filaments in different plasticizer ratios (10, 20, 30, and 40%). Shaded bars indicate the strain value in which the samples present linear viscoelastic response at (A) 200°C and (B) 0°C.

3.2.6 Preparation of printlets by FDM 3D printing

Printlets (3D printed tablets; (Goyanes et al., 2017)) were produced using two FDM 3D printers, Makerbot Replicator Mini+ (New York, NY, USA) and Voolt3D model Gi3 (São Paulo, Brazil) endowed with a nozzle diameter of 0.5 mm and 0.3 mm, respectively. To better assess the influence of each brand's printing design on the preparation of the tablets, all printer parameters were fixed. The printing temperature varied according to the concentration of plasticizer as described in Table 3.1. Ten tablets were printed at a time. The layer height was fixed at 0.2 mm, the infill density was 30%

using a rectilinear pattern, and the printing speed was 60 mm/s for printing moves and 150 mm/s for travel speed. All printlets were round and flat graphically designed and produced by Tinkercad® (Autodesk® Inc, San Rafael, CA, USA) and Slic3r® (Rome, Italy) or Makerbot Print™ softwares, and were projected with 14 mm of diameter and 4 mm of thickness. The temperature chosen for printing the tablets was around 40 °C above the temperature used for HME (Table 3.1) (Zhang et al., 2017).

3.2.7 Thermal analyses

All filaments were milled at 20,000 rpm using a Hamilton Beach knife mill (Glen Allen, VA, USA) with a stainless-steel blade of 1.6 mm thick. The resulting granules with particle size between 180–150 µm were used for the tests.

To identify Tg temperatures of the filaments, differential scanning calorimetry (DSC) was performed in a DSC-60 (Shimadzu, Tokyo, Japan) through a heating-cooling-heating cycle, from 20 to 100 °C, then from 100 to 0 °C, and finally from 0 to 150 °C at a rate of 20 °C/min, using approximately 5 mg of samples placed in aluminum pans. To eliminate any water content present in the formulation, the samples were kept at 100 °C for 10 min (first heating), and to stabilize the baseline and allow the identification of Tg even at low temperatures, a holding time of 10 min was also applied at 0 °C, before starting the second heating (Newman and Zografi, 2020).

Thermogravimetric analysis (TGA) was performed by a DTG-60H (Shimadzu, Tokyo, Japan) operating from 25 to 500 °C at a heating rate of 10 °C/min, with approximately 5 mg of samples placed in platinum pans. Additionally, the water content of each extruded filament was determined by the mass loss observed between 25–105 °C, as it is considered the loss of the water absorbed by the formulation. All analyses were carried out in a nitrogen atmosphere at a flow of 50 mL/min.

3.2.8 Morphological analysis

Morphological characteristics of filaments and printlets were assessed by optical microscopy using a stereoscope coupled to a camera at 10×, 20×, and 30× magnification. (Laborana/SZ – SZT, São Paulo, Brazil).

3.2.9 Weight uniformity and dimensions measurements

The average mass of the printlets (n = 10) was determined by an analytical balance with a readability of 0.00001 g (Shimadzu, Tokyo, Japan). The diameter and thickness of

all printlets (n = 10) were also determined by means of a digital caliper (Mitutoyo Sul Americana, São Paulo, Brazil).

2.10 Statistical analysis

The statistical analysis of the data obtained for physical and dimensional uniformity tests (filaments diameter, and tablets thickness, diameter, and weight) was performed using GraphPad Prism 8 (San Diego, CA, USA). All data showed normal distribution according to the D'agostino-Pearson normality test, showing parametric behavior. Therefore, the results were analyzed using one-way ANOVA, followed by Tukey post-test. The level of significance (p) was fixed at 0.05.

3.3. Results and discussion

3.3.1 Filament development

PVA was chosen as a polymeric matrix model for its versatility in pharmaceuticals, being used in several dosage forms such as modified-release tablets, transdermal films, and ophthalmic formulations, besides 3D biomedical devices (AZAD et al., 2020; TEODORESCU; BERCEA; MORARIU, 2019). Additionally, PVA has proven to be one of the most promising polymeric materials for FDM 3D printing of drug products, thanks to its thermal and rheological properties (PEREIRA et al., 2020). In particular, PVA is commonly processed by HME at temperatures not exceeding 180 °C and printed by FDM using temperatures of up to 200 °C (MOHANTY et al., 2016). These are safe process conditions for this material, below its initial decomposition temperature (246 °C) (Figure 3.2).

On the other hand, several plasticizers used to improve the rheological properties and facilitate the extrusion of this polymer, such as triethyl citrate (KATOPODIS et al., 2020) and GLY, shows initial degradation in a range of 130–150 °C, i.e., within the processing temperature zones used in HME and FDM 3D printing. Still, GLY was chosen as a plasticizer for this study considering its slow kinetic degradation up to 200 °C (Figure 3.2) and the reduced residence time of the samples during HME. Additionally, GLY is widely used with PVA in HME (ARIANTO et al., 2021; CHEN et al., 2020; KAHVAND; FASIHI, 2020), showing compatibility and polymer-plasticizer interactions that guarantees sample stability, even at high processing temperatures (XU et al., 2020b).
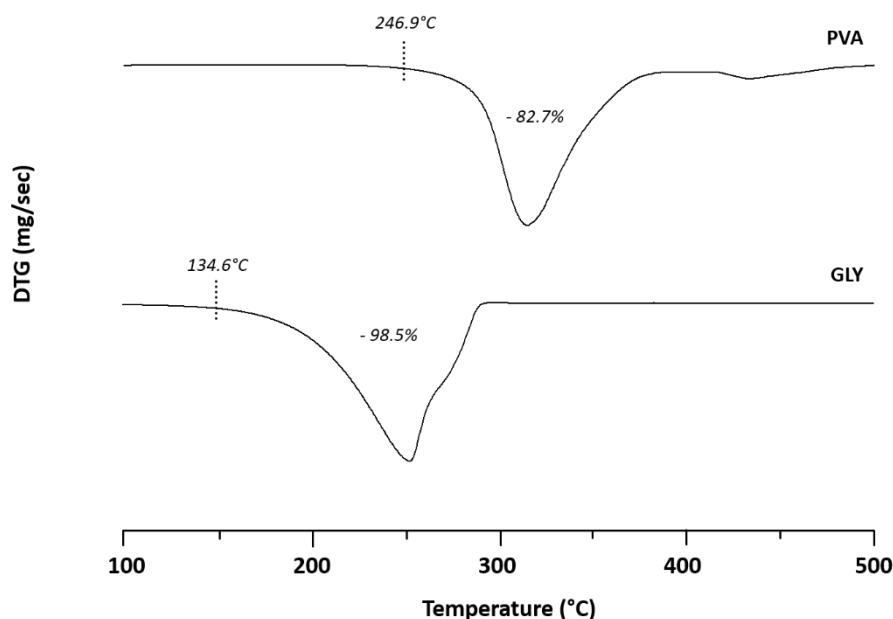
Figure 3.2 DTG curves of PVA and GLY as supplied. All mass loss events described in the range 100–500 °C are indicated in the thermograms as a percentage (%) along with the initial decomposition temperature.

PVA with different concentrations of GLY was then processed by HME to produce filaments with different rheological and mechanical patterns in order to put the herein proposed protocol to the test.

The first challenge was establishing an extrusion condition capable of preparing uniform filaments with an ideal diameter to feed FDM 3D printers without causing formulation components' degradation. For this purpose, different temperatures and rotation speeds were tested, while the extrusion torque was monitored to assess the material's processability. Torque values between 0.4–0.2 Nm were considered ideal and were used to define the extrusion parameters. Since, higher torque measurements lead to high mechanical stress, causing degradation by shear, while low values produce poor miscibility of the components (LIMA et al., 2020).

Thus, the extrusion temperatures were set individually, based on the percentage of GLY in each formulation. All extrudates produced did not show any darkening, suggesting the absence of sample degradation (Table 3.1), which was later confirmed by thermogravimetric analyses. Further, these parameters were used to select the

temperatures for the FDM 3D printing (Table 3.1), typically 40 °C above the HME temperature (ZHANG et al., 2017).

3.3.2 Filament characterization

All filaments, regardless of plasticizer ratio, showed slight variations in diameter (standard deviation ≤ 0.2), which should allow a more homogeneous feeding of the printer and a more regular deposition of layers, resulting in printlets with weight uniformity (PONSAR; WIEDEY; QUODBACH, 2020). Ideally, the diameter of the filaments for 3D printers should be in the range of 1.6 to 1.8 mm (KORTE; QUODBACH, 2018; PONSAR; WIEDEY; QUODBACH, 2020). The average thickness of PVA-GLY 10% and PVA-GLY 20% (1.60 and 1.61 mm, respectively) match such conditions (Figure 3.3), while PVA-GLY 30% and PVA-GLY 40% had mean diameter values of 1.34 and 1.38 mm, respectively; therefore, outside the recommended range.

In general, the diameter of HME filaments can be adjusted with the tractor speed, i.e., by accelerating the puller's rate, the filament becomes thinner, and by decreasing it the filament becomes thicker. However, even with the minimum tractor speed and by using a HME die with an opening of 1.8 mm, the malleability of PVA-GLY 30% and PVA-GLY 40% formulations lead to filaments outside the indicated diameter range for 3D printing.

The temperatures used in the HME favor the obtaining of products with low moisture content; however, many extrudates absorb moisture quickly, even when stored under controlled conditions (ALSHAHRANI et al., 2015; LIMA et al., 2020; OKWUOSA et al., 2021). Indeed, this hygroscopic behavior was observed for PVA-GLY filaments, especially in the samples containing more plasticizer reaching up to 7% (Table 3.1). In such case, both polymer and plasticizer are hygroscopic (AL-HAYALI; SALMAN; HADI AL-JANABI, 2021; TRIYONO et al., 2020). Still, further glycerin addition can lead to more hygroscopic formulations due to rheological alterations caused by the plasticizing effect, which rise the free volume of the amorphous region of the polymer, increasing its chains malleability, and consequently facilitating water uptake (HOSSEINI; NABID, 2020).
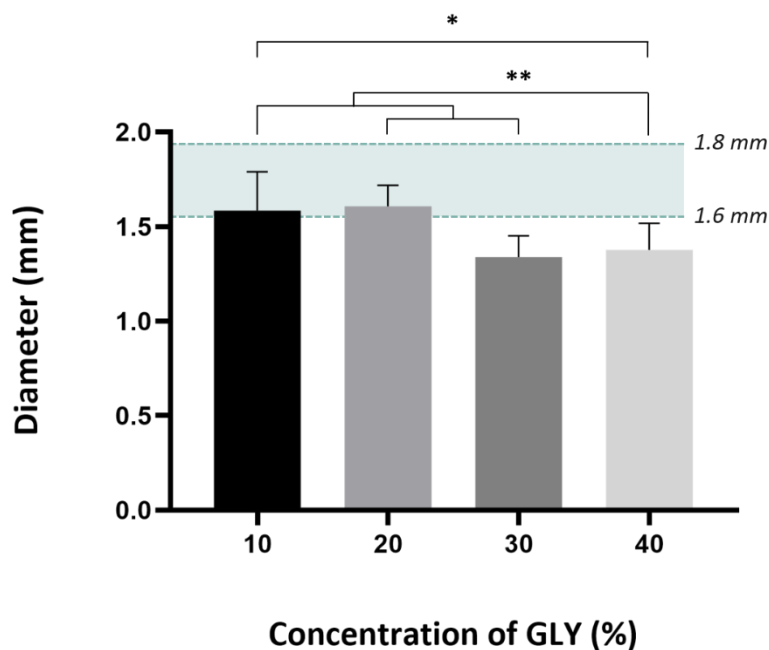
Figure 3.3 Diameter of PVA-GLY filaments in different plasticizer ratios (10, 20, 30, and 40%). The dotted region indicates the diameter range known as acceptable for a FDM 3D printer (KORTE; QUODBACH, 2018; PONSAR; WIEDEY; QUODBACH, 2020). All significant difference is represented by asterisks, where *($p < 0.05$) and **($p < 0.005$).

A water content above 2% is enough to promote a large endothermic peak in DSC curves at temperatures between 25–100 °C, which hind Tg identification, represented in this technique by a baseline drop (NEWMAN; ZOGRAFI, 2020). Hence, a heating-cooling-heating cycle was necessary to desiccate the sample and enable Tg determination by DSC. Contrary to the expected, all filaments, regardless the GLY percentage, showed similar Tg values of approximately 37 °C (Figure 3.4).

Plasticizer addition, especially at high concentrations, is expected to cause a reduction in polymer's Tg temperature (VAROL et al., 2020). In this assay, the drying step necessary to remove the interference of the water possibly modified the sample and impaired the plasticizing effect. The decisive influence of DSC samples preparation in the identification of the Tg has already been described (NEWMAN; ZOGRAFI, 2020). Such experimental bias practically makes the use of linear heating DSC unfeasible to monitor the polymers Tg. Considering such analytical uncertainty, rheological evaluations take on even greater importance as, for example, several viscoelastic variations were identified by the rheological analyses.
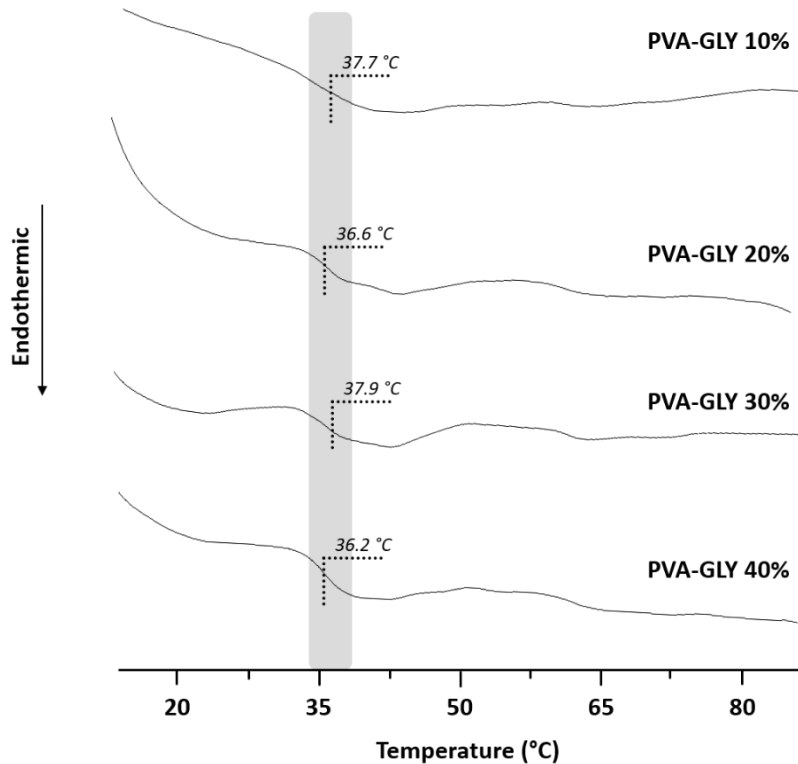
Figure 3.4 DSC curves for the second heating of PVA-GLY filaments in different plasticizer ratios (10, 20, 30, and 40%). The glass transition temperature range is shaded, and the midpoint temperature is indicated in the thermograms.

Tg determinations obtained based on tan δ of oscillatory rheology (Figure 3.5) were consistent with the expected behavior of the plasticizer effect in the PVA containing GLY proportions. This polymer alone presents a Tg of approximately 46 °C (KATOPODIS et al., 2020). PVA-GLY 10% filament showed a Tg of 43.5 °C, indicating minor GLY interference on polymer's Tg. Other studies have already identified that such amount of plasticizer may not be enough to cause significant changes in polymer Tg, even if the deformation intensity is changed (FUNG; SURYANARAYANAN, 2017; PINHO et al., 2021).

On the other hand, a meaningful shift in the Tg peak was observed for all other samples, in which the increase in plasticizer content caused an important decrease in Tg values (Figure 3.5). Such change in Tg response indicates that PVA-GLY 30% and PVA-GLY 40% are flexible filaments at room temperature since their Tg is equal to or less than 25 °C (25.6 and 16.1 °C, respectively). This characteristic may hamper the 3D printing feeding step, especially considering that the increase in plasticizer ratio also reduced the thickness of the extruded filaments, as shown in Figure 3.3.
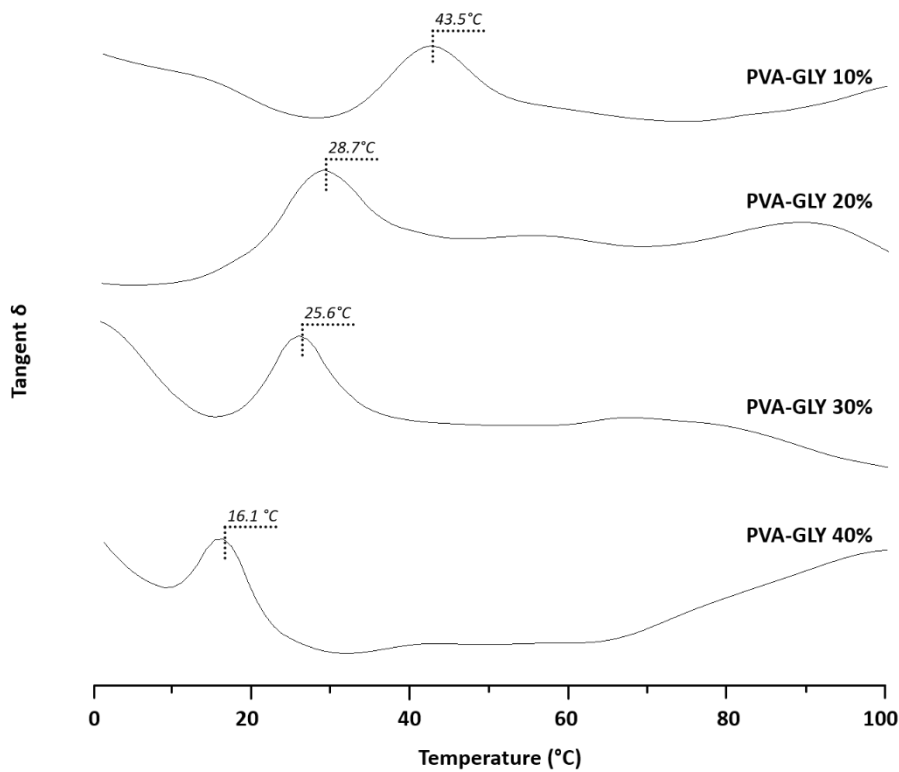
Figure 3.5 Tan δ of PVA-GLY filaments in different plasticizer ratios (10, 20, 30, and 40%). The glass transition temperature, indicated by the inflection point of tan δ, is marked in the curves by the dotted line.

In temperature ramps, the sharp drop in complex viscosity (η^*) indicates viscoelastic materials' high deformation and fluidity. Thereby, polymers that exhibit an accentuate decline on η^* at low temperatures may not be suitable for 3D printing, as they can flow too easily while not pulling correctly, clogging the nozzle, as illustrated in Figure 3.6A. On the other hand, polymers with high values of η^* are incapable of being pulled towards the nozzle since its high elasticity prevents deformation, forcing the filament to be broken (Figure 3.6B).

Thus, an adequate balance of elastic and viscous moduli is necessary to provide a proper complex viscosity that allows an adequate melt flow and ensure a correct 3D printing (Figure 3.6C). Therefore, in this delicate scenario of complex deformation for additive manufacturing, η^* values close to 0.8 kPa.s at the set printing temperature have been considered ideals for FDM 3D printing (DIEDERICHS et al., 2019).
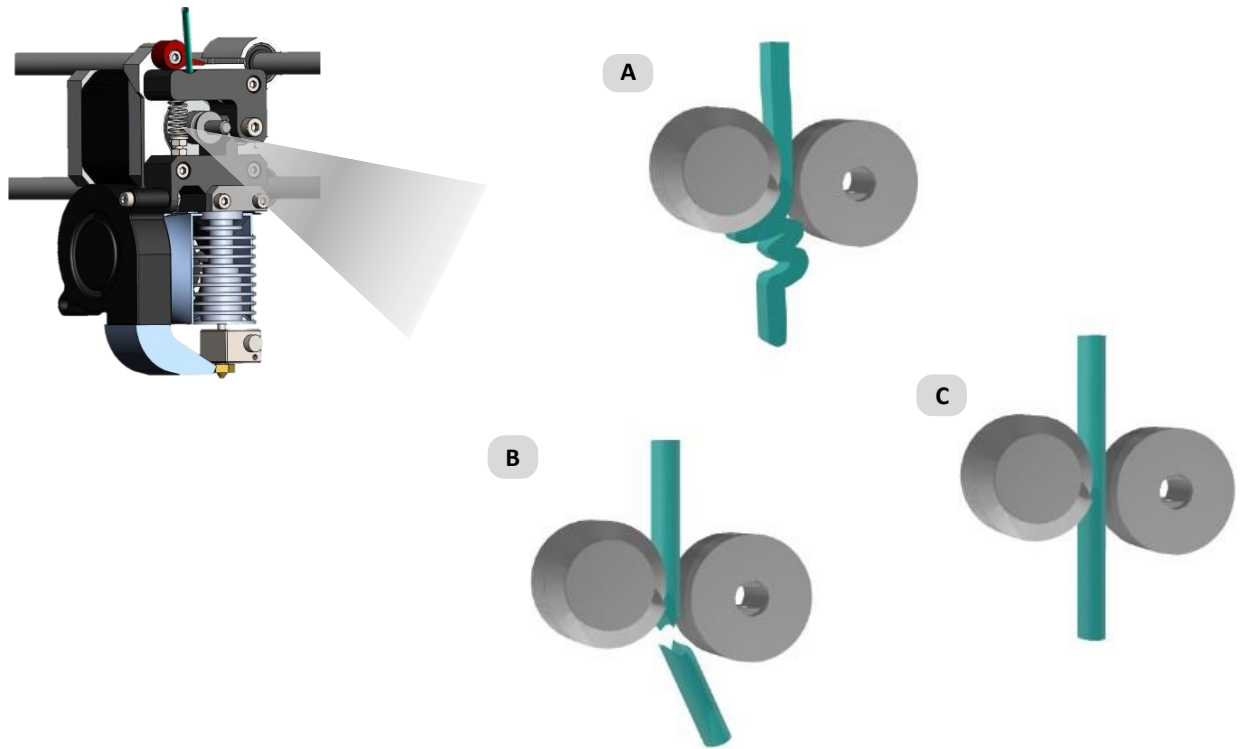
Figure 3.6 Representation of the FDM 3D printer extruder with a schematic illustration of (A) a soft filament clogging the extruder, (B) a rigid filament breaking with gear traction, and (C) a free-flowing filament.

As shown in Figure 3.7, PVA filaments with 10% and 20% GLY have viscosity values close to 0.8 kPa.s at the printing temperature (Figure 3.7, green region). This result indicates these filaments have a suitable viscosity to be pulled by the gear, flow through the nozzle, and build adequate 3D structures layer by layer.

PVA-GLY 30%, in turn, at the set temperature for printing, also has a complex viscosity near 0.8 kPA.s (Figure 3.7). However, viscosity sharp drop starts at 125 °C (Figure 3.7, gray region), which indicates that this filament starts an intense deformation process at lower temperatures. Indeed, the anticipation of this rheological behavior caused by heat can impair the traction by 3D printer since predecessor regions of the nozzle have high temperatures due to heat dissipation (YANG et al., 2021). In this way, filaments deformation starts before reaching the nozzle, which could clog the printer, especially considering this filament is thinner and more fragile than the PVA-GLY 20%.
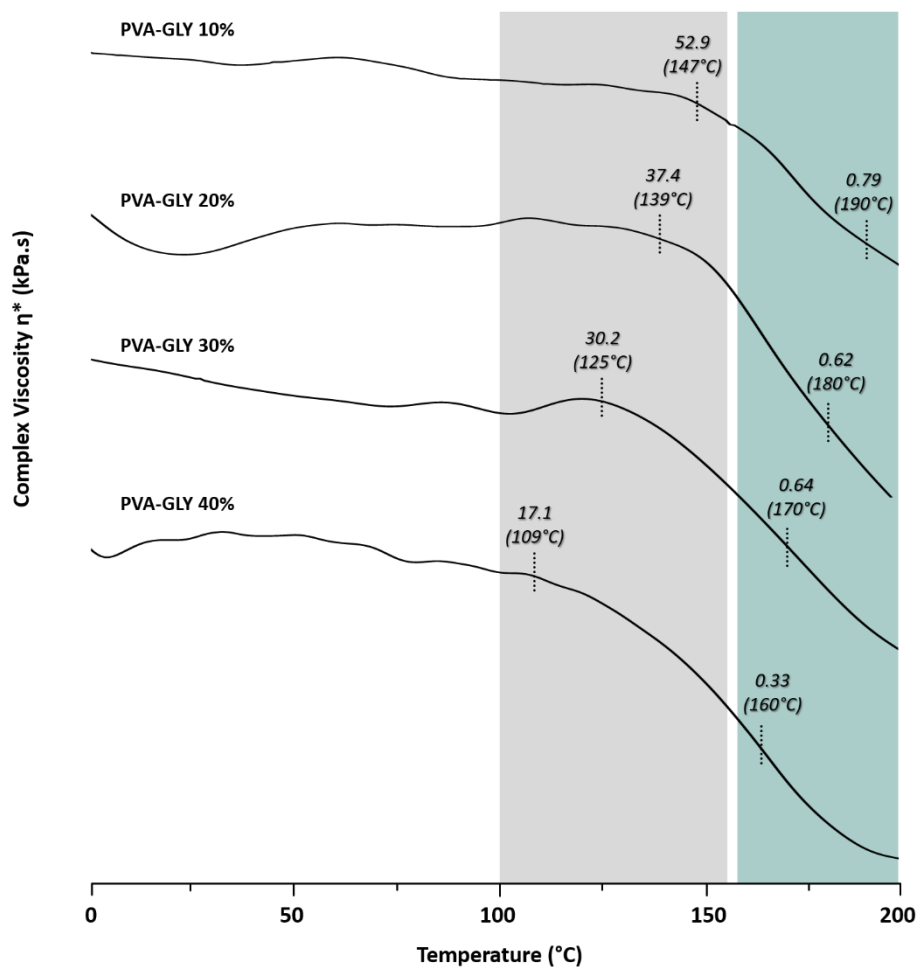
Figure 3.7 Complex viscosity (η^*) of PVA-GLY filaments in different plasticizer ratios (10, 20, 30, and 40%). Temperature and complex viscosity values for initial η^* loss are represented in a gray shaded area, and complex viscosity values at the printing temperature are indicated in the green shaded area.

Meanwhile, PVA-GLY 40% showed a complex viscosity of 0.33 kPa.s at the temperature chosen for initial printing tests, which suggests that the high malleability will clog the printer and prevent the filament from being continuously directed to the nozzle.

Besides the unfavorable viscoelastic characteristics of PVA-GLY 30% and PVA-GLY 40%, they are also extremely flexible even before reaching the gear pull step and too thin to be used in FDM 3D printers. Hence, these mixtures are unfeasible for the printing process even before the filament is heated (GOOLE; AMIGHI, 2016; KRAUSE et al., 2019; PARK et al., 2021).

Polymer-plasticizer and polymer-drug interaction can potentially produce distinct alterations in rheological and thermal properties (WEI et al., 2020). Moreover, significant

changes in Tg, viscoelastic profile, and polymer melting temperature can manifest independently (PAUL et al., 2021; SAHI; DJIDJELLI; BOUKERROU, 2021; WONG et al., 2017).

In the case of PVA-GLY filaments, the plasticizer concentration could gradually modify Tg temperature and complex viscosity profile without changing PVA crystallinity. Indeed, Figure 3.8 shows the polymer melting is around 170 °C, indicated by the temperature in which G" becomes greater than G' (CUCALON et al., 2019).
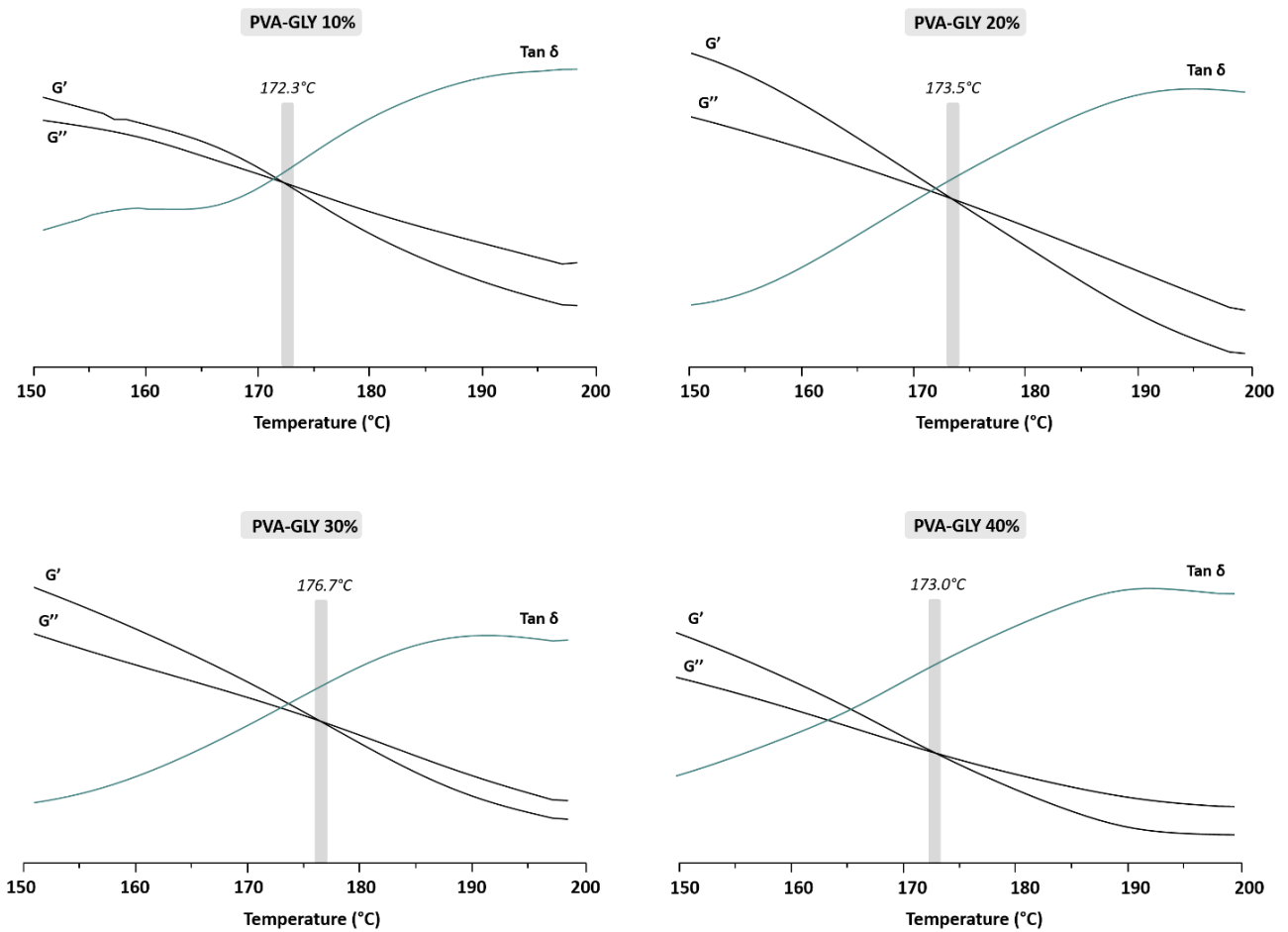
Figure 3.8 Dynamic oscillation temperature ramp of PVA-GLY filaments in different plasticizer ratios (10, 20, 30, and 40%). The rheological patterns G', G" and tan δ are plotted, and the crossover temperature (G' = G") are indicated and shaded in gray.

The melting point of PVA, a semicrystalline polymer, did not change with the plasticizer, which is corroborated by the literature (ANDRADE; GONZÁLEZ-MARTÍNEZ; CHIRALT, 2021; BOONSUK et al., 2020). This behavior is commonly

observed in semicrystalline polymers since the plasticizing effect frequently consists in swelling the amorphous region of the polymer, increasing the free volume between molecular chains, which decrease Tg and melt viscosity, while keeping the crystalline regions unchanged (LIM; HOAG, 2013).

Maintaining the crystalline profile of the polymer ensures that the resistance of the filament will be less affected, since crystallinity is known to impart the strength needed for a FDM printing material (LI et al., 2018). Thus, as the polymer-plasticizer interaction caused intense modifications in the amorphous region of PVA, it is interesting that the polymer maintains its crystalline characteristics unaltered to control chains deformation, especially for the PVA-GLY 10% and PVA-GLY 20% filaments, as their viscosity was identified within the accepted zone for 3D printing (Figure 3.7).

Another important parameter to be considered when evaluating filaments to be used in a FDM 3D printer is the polymer recovery after molten deformation. Thus, suitable tablets are obtained not only when HME and 3D printing processes are successful since the post-printing step must also be effective to ensure adequate structuring and stability of drug products (ALHIJJAJ; BELTON; QI, 2016).

Complex modulus (G*) describes the entire viscoelastic behavior of a sample as it is the measure of the deformation resistance. Table 3.2 shows the printing temperature, PVA-GLY 10% has low resistance to deformation, being able to flow easily through the printer nozzle. The other filaments, in turn, have lower G* values, suggesting that these samples could flow extremely easily through the nozzle, depositing more material than necessary.

Moreover, G* values at room temperature (25 °C) can provide information about the solidification of the printlets after the entire printing process, especially considering that the values given in Table 3.2 were obtained with a decreasing temperature ramp analysis. PVA-GLY 10% and PVA-GLY 20% have a high complex modulus, which indicates that the printed tablets will have a rigid structure at 25 °C, while the PVA-GLY 30% and PVA-GLY 40% filaments will produce flexible and malleable tablets.

Rigid structures tend to present better shelf-life stability since flexible objects that deform very easily are more susceptible to physical and chemical variations when subjected to strict environmental conditions, such as storage temperature and humidity (OKWUOSA et al., 2021).

Table 3.2 Complex modulus (G*) at room temperature (25 °C), and in the temperatures used in the hot-melt extrusion (HME) and 3D printing (3DP) process, along with the average fracture force (N) ± standard deviations of the filaments (n = 5).

Formulation	Rheology at room temperature	Rheology at HME temperature	Rheology at 3DP temperature	Mechanical properties
	G* (*MPa*)	G* (*MPa*)	G* (*MPa*)	Fracture force (*N*)
PVA-GLY 10%	1.08	0.13	0.0064	28.1 ± 1.2
PVA-GLY 20%	0.63	0.14	0.0043	16.2 ± 2.9
PVA-GLY 30%	0.28	0.12	0.0040	6.6 ± 1.8
PVA-GLY 40%	0.16	0.04	0.0021	3.2 ± 0.6

Besides temperature dependence, mechanical pressure also has an important influence on materials' deformation. When a tensile force is exerted on a solid material, its chemical bonds stretch(SAMARO et al., 2020). Then, when the stress is removed, the intra-atomic bonds can relax and recover, returning to their original form (elastic deformation) or being irreversibly destroyed and maintaining its new conformation (plastic deformation) (TANG; FUJIMOTO; OKAZAKI, 2020). Therefore, polymeric filaments' toughness and molecular malleability are dominant properties that allow gear traction and good feedability in a FDM 3D printer (HENRY et al., 2021; XU et al., 2020a).

Accordingly, stress-strain tensile tests were performed to determine the mechanical properties of the filaments (Figure 3.9). In this characterization, the first part of the curve is formed by a linear growth, corresponding to elastic deformation, followed by a necking behavior, in which there are few changes in stress causing marked variation in strain, related to plastic deformation (Figure 3.9A) (ALHARBI; KONG; PATEL, 2020).
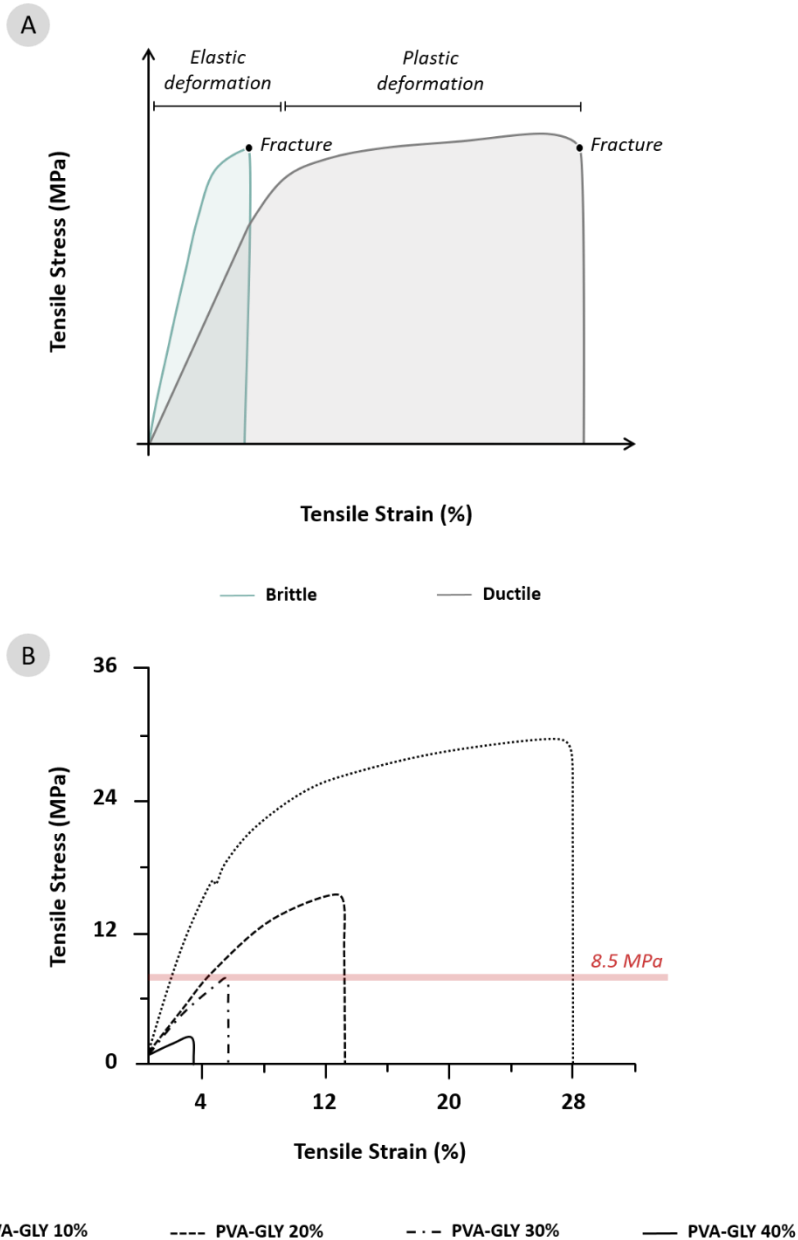
Figure 3.9 Hypothetical stress–strain curves (**A**) indicating elastic and plastic deformation, toughness (area under the curve), and fracture point of brittle (fragile) and ductile (resistant) materials; and (**B**) experimental curves of PVA-GLY filaments containing different plasticizer ratios (10, 20, 30, and 40%). The red dotted line marks the lower stress limit described in the literature for 3D FDM filaments.

Figure 3.9B shows that PVA-GLY 10% is the only sample that has a long plastic deformation and a large area under the curve, which indicates, respectively, that this material is ductile and has high toughness, characteristics required for adequate traction provided by a 3D printer (XU et al., 2020a; YANG et al., 2021). Concurrently, PVA-GLY 20% is less resistant but has a medium fracture force (Table 3.2), being able to

withstand the pressure of the 3D printer gear. Breaking stress values higher than 8.5 MPa has been described for filaments capable of supporting the traction of a FDM 3D printer (YANG et al., 2021). In contrast, PVA-GLY 30% and PVA-GLY 40% have an extremely fragile and brittle behavior, as these filaments did not present plastic deformation, consequently supporting little stress (Fig 7B) and fracturing with small forces (Table 3.2).

Furthermore, since PVA has sufficient mechanical properties to deform with low stress values, none of the samples proved to be tough and ductile enough to avoid stress deformation promoted by gears traction. These results confirm the ease adaptation of this polymer to produce drug products by HME-3D techniques, comparing to other pharmaceutical polymers, which tend to produce rigid filaments with poor malleability (YANG et al., 2021).

3.3.3 Printlets characterization and protocol checking

The oscillatory shear rheological analysis allowed to identify that PVA-GLY 10% and PVA-GLY 20% filaments are potentially suitable for FDM 3D printing since both exhibited appropriate diameter, mechanical, and rheological properties to withstand the stress provided by the printing process and still form stable objects with the characteristics expected for drug products. Contrarily, filaments with 30% and 40% plasticizer ratios may not be appropriate for 3D printing since they do not put together the characteristics to ensure good feedability and printability.

The differences that can be found in FDM 3D printers also play an important role. Generic FDM 3D printers have a basic mechanism of mechanical operation, formed by a short and straight traction system with regular nozzle movements, as in the Voolt3D printer used in this study. Some manufacturers have implemented modifications to this mechanical arrangement to make it more efficient and increase the accuracy level in the printing of objects (GOOLE; AMIGHI, 2016).

In the case of the Makerbot Replicator Mini+ printer, also used in this study, such modifications involve a long run of the extrusion process that avoids clogging, movement sensors capable of improving the definition of the 3D object, and an accelerated cooling mechanism that facilitates polymer recovery and solidification (HENRY et al., 2021; ZI et al., 2019). In practice, such modifications make these printers more sensitive to changes in the viscoelasticity of the filaments, as well as to variations in their diameter (GÜLTEKIN et al., 2021).

Therefore, printers with a more conventional design, such as Voolt3D, are known to accept filaments with various viscoelastic properties and diameters; however, do not elaborate structures as precisely as MakerBot (PIRES et al., 2020; ZI et al., 2019). Furthermore, the printer brand, the nozzle die size, and modifications in filament formulation are already known to promote a significant impact on the mass and dimensions of the final 3D (BERAN et al., 2018; GENDVILIENE et al., 2020; HENRY et al., 2021; KRAUSE et al., 2019; PIRES et al., 2020). Indeed, PVA-GLY 10%, PVA-GLY 20%, and PVA-GLY 30% filaments could be printed by Voolt3D, while only the filaments with 10% and 20% of plasticizer could feed MakerBot printer and produce tablets.

Thermogravimetric analyzes showed filaments with GLY in the range of 10–30% presented two decomposition stages that coincide with the sum of mass loss phases of their individual compounds (Figure 3.10), i.e., the first stage related to GLY degradation and the second one correspondent to PVA (Figure 3.2). Additionally, the initial temperature of the second decomposition peak is shifted to lower temperatures indicating an interaction between polymer and plasticizer after the HME process and especially after 3D printing, as this modification is even more intense in tablets' decomposition profile (Figure 3.10).

These interactions were responsible for delaying the decomposition of a part of GLY present in the sample since the first peak of the TGA curve has a mass loss percentage lower than expected, and the second peak corresponds to an amount of decomposed mass greater than the amount of polymer that degrades in this temperature range (Figure 3.2). This behavior is even more intense as the amount of plasticizer increases, especially for the PVA-GLY 40% filament, in which it is possible to identify several decomposition phases, and for PVA-GLY 30% tablet, where an intermediate peak between 200-300 °C was observed (Figure 3.10).

Photographs for morphological analysis of all filaments that could be printed on both selected additive manufacture machines is exhibited in Figure 3.11. No signs of darkening that could be related to degradation were identified. Additionally, PVA-GLY 10% filament produced uniform structures with well-developed shell and infill in both tested printers. Differently, PVA-GLY 20% produced homogeneous and consistent tablets only in Voolt3D (Figure 3.11A). The infill thickness of tablets obtained by MakerBot was greater than expected (Figure 3.11B).
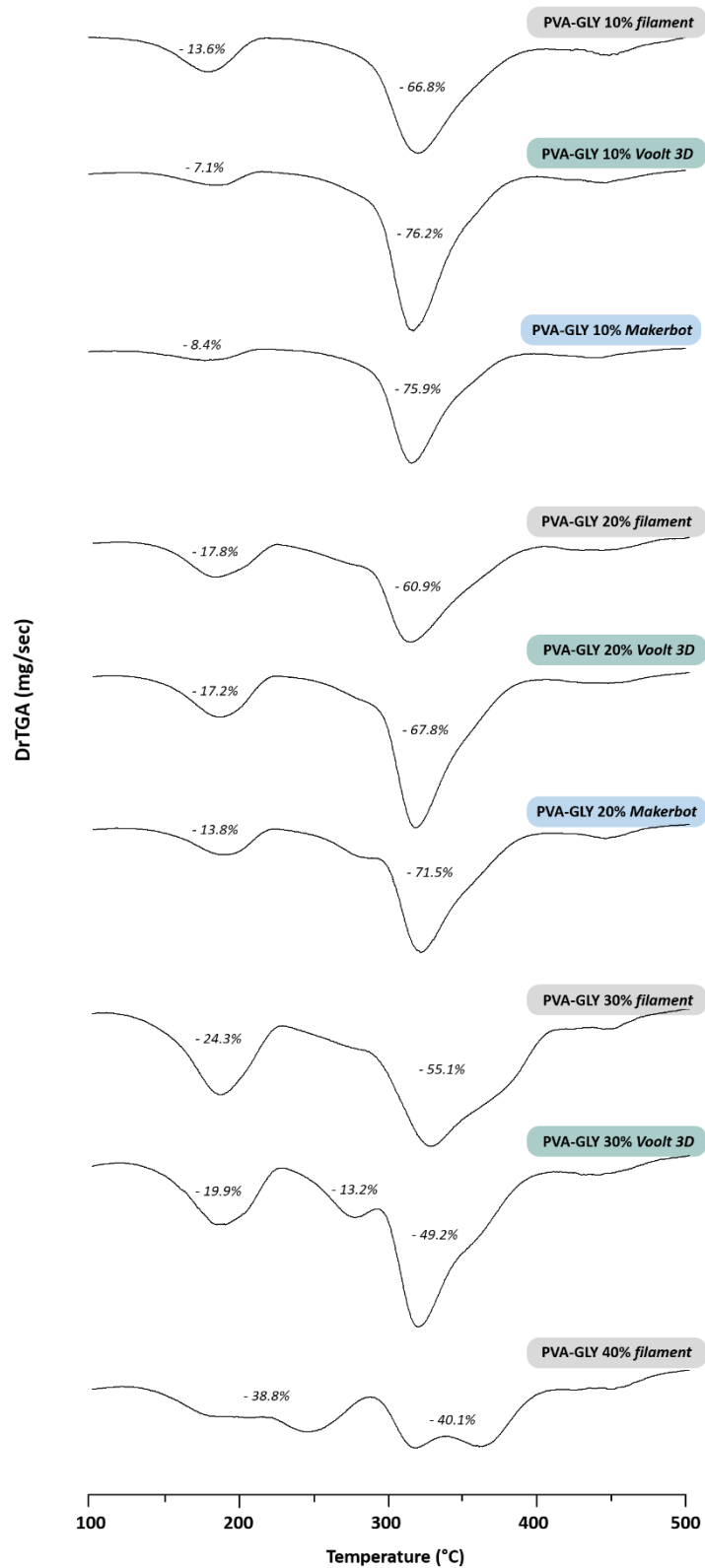
Figure 3.10 DTG curves of PVA-GLY filaments in different plasticizer ratios (10, 20, 30, and 40%) and their printlets produced by Voolt3D and MakerBot. All weight loss described in the range 100 – 500 °C is indicated in the thermograms as a percentage (%).

This modification observed in MakerBot's printlets confirmed the hypotheses pointed after rheological evaluation. As the viscosity of PVA-GLY 20% is lower than PVA-GLY 10% filament (Figure 3.7), its molten deformation is more intense and accelerated at printing temperature (Table 3.2), causing greater amounts of material to flow through the nozzle and be deposited on the constructed object, forming heterogeneous inner structures using this printer.
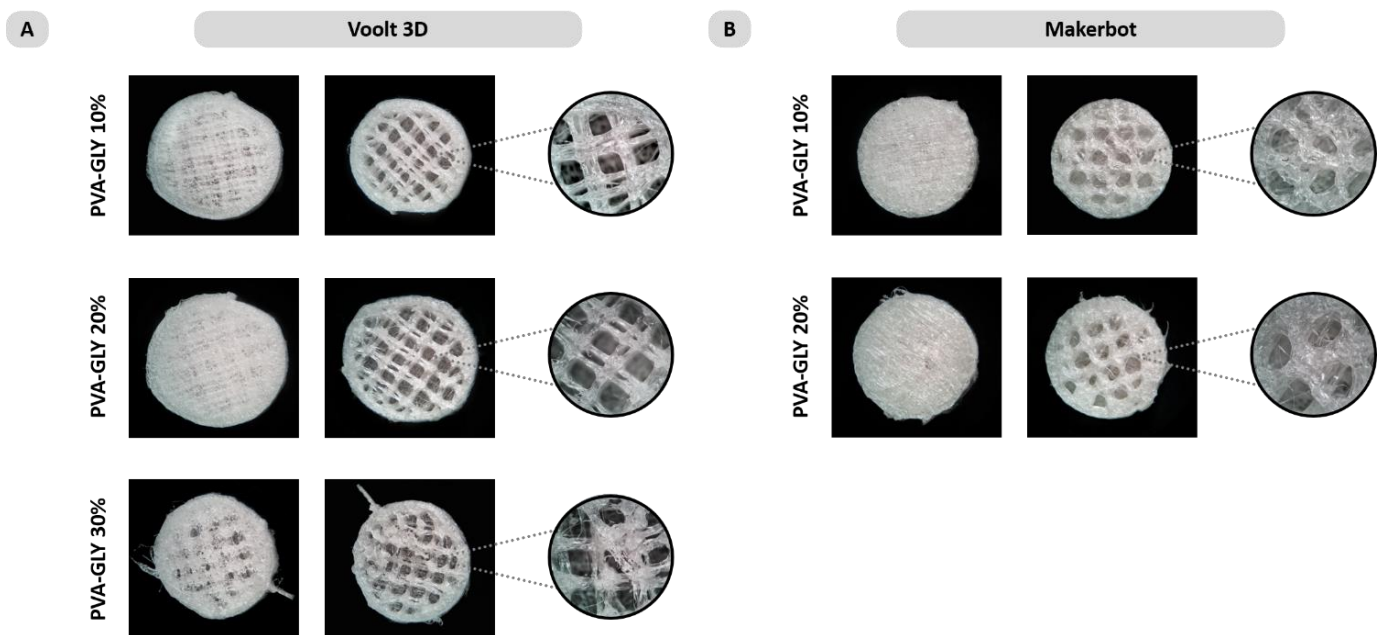
Figure 3.11 Optical microscopy of tablets' outer and inner portion produced by (A) Voolt3D and (B) MakerBot at a 10 and 30× magnification.

Tablets elaborated with PVA-GLY 30% (only possible in Voolt3D) had significant failures in shell and infill construction (Figure 3.11A). This result corroborates the findings of the in-process mechanical and rheological protocol proposed here. The high flexibility and thin diameter of this filament hampered it from being correctly pulled and flowing steadily into the nozzle, creating solid and irregular structures around the tablet (Figure 3.11A). In addition, the lack of elastic component in this sample hindered polymer recovery, making this tablet flexible at room temperature, as suggested by its low G* value (Table 3.2).

In terms of pharmaceutical performance, intense modifications and inaccuracies in printlets morphology can reverberate dramatically in drug's dissolution, since porosity, size, shape, inner, and outer layers are designed in a 3D pharmaceutical dosage form to

establish the drug release profile and consequently its bioavailability (CUNHA-FILHO et al., 2017).

Table 3.3 shows the weight distribution and dimensions (diameter and thickness) of the printlets produced by each filament using different printers. The increase in GLY concentration led to heavier tablets due to an increase in the filament density that occurs from the plasticizing effect (IBRAHIM et al., 2019).

Table 3.3 Average weight (mg), diameter (mm), and thickness (mm) of tablets produced with PVA-GLY filaments in different plasticizer proportions (10, 20, and 30%) using Voolt3D or MakerBot printers. Values are expressed as mean $\pm$ standard deviations; for weight measurements, coefficient of variation is also included (in parentheses). The significant difference between tablets produced using the different printers with the same polymer-plasticizer composition is represented by asterisks, where **** ($p < 0.0001$).

Formulation	Voolt3D			MakerBot		
	Weight (*mg*)	Diameter (*mm*)	Thickness (*mm*)	Weight (*mg*)	Diameter (*mm*)	Thickness (*mm*)
PVA-GLY 10%	299.1 $\pm$ 7.6 (2.5%) ****	13.3 $\pm$ 0.09	3.9 $\pm$ 0.03 ****	367.1 $\pm$ 6.6 (1.7%) ****	13.4 $\pm$ 0.06	4.6 $\pm$ 0.06 ****
PVA-GLY 20%	318.6 $\pm$ 9.4 (2.9%) ****	13.7 $\pm$ 0.05 ****	3.9 $\pm$ 0.05 ****	475.1 $\pm$ 10.2 (2.1%) ****	13.2 $\pm$ 0.06 ****	4.6 $\pm$ 0.32 ****
PVA-GLY 30%	338.2 $\pm$ 18.7 (5.5%)	13.7 $\pm$ 0.39	3.9 $\pm$ 0.08	*na*	*na*	*na*

na: not assessed.

As the composition differences between the PVA-GLY 10 and 20% filaments are small, similar weight and dimensions results would be expected between the objects printed with such filaments. However, this only occurred in the Volt3D printer (Table 3.3). In this printer, the difference in weight between tablets printed with PVA-GLY 10 and 20% was only 6%. In contrast, in tablets printed with the Makerbot, weight variation between the filaments was 28%.

This difference in printers performance could be explained by the rheological changes between the filament and the greater sensitivity of the Makerbot printer to the filament viscoelasticity. In fact, increased molten deformation leads to more material

being deposited by the printer nozzle. Thus, it appears that the weight of the printlets and, consequently, the dosage of the drug is conditioned by the rheology of the sample, with greater influence on the printer used.

In a pharmaceutical scenario, drug dose uniformity is essential; therefore, mass coefficient of variation is a crucial parameter. All tablets produced by PVA-GLY 10% and PVA-GLY 20%, in both printers, remained with the coefficient of variation within the pharmacopoeia limits set for tablets over 250 mg ($< 5\%$) (WHO (WORLD HEALTH ORGANIZATION), 2019). PVA-GLY 30% Voolt3D tablets had a coefficient of variation above acceptable (Table 3.3), leading to inaccurate doses and changes in pharmaceutical performance. Thus, tablets obtained would not meet the pharmaceutical requirements to be dispensed to patients.

Moreover, diameter and thickness variations of all printlets was minimal (Table 3.3). Thus, the observed weight variation is not related to the size of the 3D structure but rather to the amount of material deposited internally, i.e., the thickness of the infill, as seen in Figure 3.11.

3.4. Conclusion

Oscillatory shear rheology was successfully used in the characterization of hot-melt extruded filaments. Additionally, the formulations developed with variations in plasticizer ratio provided evident viscoelastic modifications capable of validating the proposed analytical protocol. Indeed, the rheological assays were able to identify with great sensitivity viscoelastic alterations with direct repercussions on the printed tablets and their quality control parameters.

PVA filaments with 10 and 20% GLY showed a suitable viscous behavior to guarantee adequate flow through the printer nozzle. Their elastic component, in turn, was presented to control deformation and prevent extrusion clogging or 3D structures formed with flaws and inaccuracies. Moreover, the complex modulus rheological variable was essential to assess and predict the post-printing repercussions of the developed tablets, and the mechanical properties were indispensable to determine the feedability of the filaments.

3.5 Acknowledgment

3.6 References

AHO, J.; BOETKER, J. P.; BALDURSDOTTIR, S.; RANTANEN, J. Rheology as a tool for evaluation of melt processability of innovative dosage forms. **International Journal of Pharmaceutics**, v. 494, n. 2, p. 623–642, 2015.

ALHARBI, M.; KONG, I.; PATEL, V. I. Simulation of uniaxial stress–strain response of 3D-printed polylactic acid by nonlinear finite element analysis. **Applied Adhesion Science**, v. 8, n. 1, p. 1–10, 2020.

AL-HAYALI, S. K.; SALMAN, A. M.; HADI AL-JANABI, A. Effect of hygroscopic polymer-coatings on the performance of relative humidity sensor based on macro-bend single-mode fiber. **Optical Fiber Technology**, v. 62, p. 102460, 2021.

ALHIJJAJ, M.; BELTON, P.; QI, S. An investigation into the use of polymer blends to improve the printability of and regulate drug release from pharmaceutical solid dispersions prepared via fused deposition modeling (FDM) 3D printing. **European Journal of Pharmaceutics and Biopharmaceutics**, v. 108, p. 111–125, 2016.

ALSHAHRANI, S. M.; MOROTT, J. T.; ALSHETAILI, A. S.; TIWARI, R. V.; MAJUMDAR, S.; REPKA, M. A. Influence of degassing on hot-melt extrusion process. **European Journal of Pharmaceutical Sciences**, v. 80, p. 43–52, 2015.

ANDRADE, J.; GONZÁLEZ-MARTÍNEZ, C.; CHIRALT, A. Effect of phenolic acids on the properties of films from Poly (vinyl alcohol) of different molecular characteristics. **Food Packaging and Shelf Life**, v. 29, p. 100711, 2021.

ARIANTO, D.; EDIKRESNHA, D.; SUCIATI, T.; KHAIRURRIJAL. The initial study of polyvinyl alcohol/honey/glycerin composite fibers. **Materials Today: Proceedings**, v. 44, p. 3408–3411, 2021.

AZAD, M. A.; OLAWUNI, D.; KIMBELL, G.; BADRUDDOZA, A. Z.; HOSSAIN, S.; SULTANA, T. Polymers for Extrusion-Based 3D Printing of Pharmaceuticals: A Holistic Materials–Process Perspective. **Pharmaceutics**, v. 12, n. 2, p. 124, 2020.

BERAN, T.; MULHOLLAND, T.; HENNING, F.; RUDOLPH, N.; OSSWALD, T. A. Nozzle clogging factors during fused filament fabrication of spherical particle filled polymers. **Additive Manufacturing**, v. 23, p. 206–214, 2018.

BERTOLINO, M.; BATTEGAZZORE, D.; ARRIGO, R.; FRACHE, A. Designing 3D printable polypropylene: Material and process optimisation through rheology. **Additive Manufacturing**, v. 40, p. 101944, 2021.

BOONSUK, P.; SUKOLRAT, A.; KAEWTATIP, K.; CHANTARAK, S.; KELARAKIS, A.; CHAIBUNDIT, C. Modified cassava starch/poly(vinyl alcohol) blend films plasticized by glycerol: Structure and properties. **Journal of Applied Polymer Science**, v. 137, n. 26, p. 48848, 2020.

CASTRO, B. M. et al. Machine learning predicts 3D printing performance of over 900 drug delivery systems. **Journal of Controlled Release**, v. 337, p. 530–545, 2021.

CHEN, D. et al. Preparation and In vitro Evaluation of FDM 3D-Printed Ellipsoid-Shaped Gastric Floating Tablets with Low Infill Percentages. **AAPS PharmSciTech**, v. 21, n. 1, p. 1–13, 2020.

CUCALON, L. G.; KASEER, F.; ARÁMBULA-MERCADO, E.; MARTIN, A. E.; MORIAN, N.; POURNOMAN, S.; HAJJ, E. The crossover temperature: significance and application towards engineering balanced recycled binder blends. **Road Materials and Pavement Design**, v. 20, n. 6, p. 1391–1412, 2019.

CUNHA-FILHO, M.; ARAÚJO, M. R.; GELFUSO, G. M.; GRATIERI, T. FDM 3D printing of modified drug-delivery systems using hot melt extrusion: a new approach for individualized therapy. **Therapeutic Delivery**, v. 8, n. 11, p. 957–966, 2017.

DIEDERICHS, E. V.; PICARD, M. C.; CHANG, B. P.; MISRA, M.; MIELEWSKI, D. F.; MOHANTY, A. K. Strategy To Improve Printability of Renewable Resource-Based Engineering Plastic Tailored for FDM Applications. **ACS Omega**, v. 4, n. 23, p. 20297–20307, 2019.

DKIER, M.; YOUSFI, M.; LAMNAWAR, K.; MAAZOUZ, A. Chemo-rheological studies and monitoring of high-Tg reactive polyphtalamides towards a fast innovative RTM processing of fiber-reinforced thermoplastic composites. **European Polymer Journal**, v. 120, p. 109227, 2019.

FUNG, M. H.; SURYANARAYANAN, R. Use of a Plasticizer for Physical Stability Prediction of Amorphous Solid Dispersions. **Crystal Growth & Design**, v. 17, n. 8, p. 4315–4325, 2017.

GENDVILIENE, I.; SIMOLIUNAS, E.; REKSTYTE, S.; MALINAUSKAS, M.; ZALECKAS, L.; JEGELEVICIUS, D.; BUKELSKIENE, V.; RUTKUNAS, V. Assessment of the morphology and dimensional accuracy of 3D printed PLA and PLA/HAp scaffolds. **Journal of the Mechanical Behavior of Biomedical Materials**, v. 104, p. 103616, 2020.

GOOLE, J.; AMIGHI, K. 3D printing in pharmaceutics: A new tool for designing customized drug delivery systems. **International Journal of Pharmaceutics**, v. 499, n. 1–2, p. 376–394, 2016.

GOYANES, A.; FINA, F.; MARTORANA, A.; SEDOUGH, D.; GAISFORD, S.; BASIT, A. W. Development of modified release 3D printed tablets (printlets) with pharmaceutical excipients using additive manufacturing. **International Journal of Pharmaceutics**, v. 527, n. 1–2, p. 21–30, 2017.

GÜLTEKIN, H. E.; TORT, S.; TUĞCU-DEMIRÖZ, F.; ACARTÜRK, F. 3D printed extended release tablets for once daily use: An in vitro and in vivo evaluation study for a personalized solid dosage form. **International Journal of Pharmaceutics**, v. 596, p. 120222, 2021.

HARYŃSKA, A.; CARAYON, I.; KOSMELA, P.; SZELISKI, K.; ŁAPIŃSKI, M.; POKRYWCZYŃSKA, M.; KUCIŃSKA-LIPKA, J.; JANIK, H. A comprehensive evaluation of flexible FDM/FFF 3D printing filament as a potential material in medical application. **European Polymer Journal**, v. 138, p. 109958, 2020.

HENRY, S.; SAMARO, A.; MARCHESINI, F. H.; SHAQOUR, B.; MACEDO, J.; VANHOORNE, V.; VERVAET, C. Extrusion-based 3D printing of oral solid dosage forms: Material requirements and equipment dependencies. **International Journal of Pharmaceutics**, v. 598, p. 120361, 2021.

HOSSEINI, M. S.; NABID, M. R. Synthesis of chemically cross-linked hydrogel films based on basil seed (Ocimum basilicum L.) mucilage for wound dressing drug delivery applications. **International Journal of Biological Macromolecules**, v. 163, p. 336–347, 2020.

IBRAHIM, M. I. J.; SAPUAN, S. M.; ZAINUDIN, E. S.; ZUHRI, M. Y. M. Physical, thermal, morphological, and tensile properties of cornstarch-based films as affected by different plasticizers. **International Journal of Food Properties**, v. 22, n. 1, p. 925–941, 2019.

KAHVAND, F.; FASIHI, M. Microstructure and physical properties of thermoplastic corn starch foams as influenced by polyvinyl alcohol and plasticizer contents. **International Journal of Biological Macromolecules**, v. 157, p. 359–367, 2020.

KATOPODIS, K.; KAPOURANI, A.; VARDAKA, E.; KARAGIANNI, A.; CHORIANOPOULOU, C.; KONTOGIANNOPOULOS, K. N.; BIKIARIS, D. N.; KACHRIMANIS, K.; BARMPALEXIS, P. Partially hydrolyzed polyvinyl alcohol for fusion-based pharmaceutical formulation processes: Evaluation of suitable plasticizers. **International Journal of Pharmaceutics**, v. 578, p. 119121, 2020.

KORTE, C.; QUODBACH, J. Formulation development and process analysis of drug-loaded filaments manufactured via hot-melt extrusion for 3D-printing of medicines. **Pharmaceutical Development and Technology**, v. 23, n. 10, p. 1117–1127, 2018.

KRAUSE, J.; BOGDAHN, M.; SCHNEIDER, F.; KOZIOLEK, M.; WEITSCHIES, W. Design and characterization of a novel 3D printed pressure-controlled drug delivery system. **European Journal of Pharmaceutical Sciences**, v. 140, p. 105060, 2019.

LI, G.; ZHAO, J.; WU, W.; JIANG, J; WANG, B.; JIANG, H.; FUH, J. Effect of Ultrasonic Vibration on Mechanical Properties of 3D Printing Non-Crystalline and Semi-Crystalline Polymers. **Materials**, v. 11, n. 5, p. 826, 2018.

LIM, H.; HOAG, S. W. Plasticizer Effects on Physical–Mechanical Properties of Solvent Cast Soluplus® Films. **AAPS PharmSciTech**, v. 14, n. 3, p. 903–910, 2013.

LIMA, A. L.; PINHO, L. A. G.; CHAKER, J. A.; SA-BARRETO, L. L.; MARRETO, R. N.; GRATIERI, T.; GELFUSO, G. M.; CUNHA-FILHO, Marcilio. Hot-Melt Extrusion as an Advantageous Technology to Obtain Effervescent Drug Products. **Pharmaceutics**, v. 12, n. 8, p. 779, 2020.

MOHANTY, S.; SANGER, K.; HEISKANEN, A.; TRIFOL, J.; SZABO, P.; DUFVA, M.; EMNÉUS, J.; WOLFF, A. Fabrication of scalable tissue engineering scaffolds with dual-pore microarchitecture by combining 3D printing and particle leaching. **Materials Science and Engineering: C**, v. 61, p. 180–189, 2016.

NEWMAN, A.; ZOGRAFI, G. Commentary: Considerations in the Measurement of Glass Transition Temperatures of Pharmaceutical Amorphous Solids. **AAPS PharmSciTech**, v. 21, n. 1, p. 1–13, 2020.

OKWUOSA, T. C.; SADIA, M.; ISREB, A.; HABASHY, R.; PEAK, M.; ALHNAN, M. A. Can filaments be stored as a shelf-item for on-demand manufacturing of oral 3D printed tablets? An initial stability assessment. **International Journal of Pharmaceutics**, v. 600, p. 120442, 2021.

PARK, S. J. et al. Additive manufacturing of the core template for the fabrication of an artificial blood vessel: the relationship between the extruded deposition diameter and the filament/nozzle transition ratio. **Materials Science and Engineering: C**, v. 118, p. 111406, 2021.

PAUL, U. C.; FRAGOULI, D.; BAYER, I. S.; ZYCH, A.; ATHANASSIOU, A. Effect of Green Plasticizer on the Performance of Microcrystalline Cellulose/Polylactic Acid Biocomposites. **ACS Applied Polymer Materials**, v. 3, n. 6, p. 3071–3081, 2021.

PEREIRA, G. G.; FIGUEIREDO, S.; FERNANDES, A. I.; PINTO, J. F. Polymer Selection for Hot-Melt Extrusion Coupled to Fused Deposition Modelling in Pharmaceutics. **Pharmaceutics**, v. 12, n. 9, p. 795, 2020.

PINHO, L. A. G.; LIMA, A. L.; SA-BARRETO, L. L.; GRATIERI, T.; GELFUSO, G.; MARRETO, R. N.; CUNHA-FILHO, M. Preformulation studies to guide the production of medicines by fused deposition modeling 3D printing. **AAPS PharmSciTech**, 2021.

PIRES, F. Q.; ALVES-SILVA, I.; PINHO, L. A. G.; CHAKER, J. A.; SA-BARRETO, L. L.; GELFUSO, G. M.; GRATIERI, T.; CUNHA-FILHO, M. Predictive models of FDM 3D printing using experimental design based on pharmaceutical requirements for tablet production. **International Journal of Pharmaceutics**, v. 588, p. 119728, 2020.

PONSAR, H.; WIEDEY, R.; QUODBACH, J. Hot-Melt Extrusion Process Fluctuations and Their Impact on Critical Quality Attributes of Filaments and 3D-Printed Dosage Forms. **Pharmaceutics**, v. 12, n. 6, p. 511, 2020.

RABBANI, A.; SCHMITT, D. R. Ultrasonic shear wave reflectometry applied to the determination of the shear moduli and viscosity of a viscoelastic bitumen. **Fuel**, v. 232, p. 506–518, 2018.
SADEGHI-MEHR, A.; RAUDSEPP, P.; BRÜGGEMANN, D. A.; LAUTENSCHLAEGER, R.; DRUSCH, S. Dynamic rheology, microstructure and texture properties of model porcine meat batter as affected by different cold-set binding systems. **Food Hydrocolloids**, v. 77, p. 937–944, 2018.

SAHI, S.; DJIDJELLI, H.; BOUKERROU, A. Study of the properties and biodegradability of the native and plasticized corn flour-filled low density polyethylene composites for food packaging applications. **Materials Today: Proceedings**, v. 36, p. 67–73, 2021.

SAMARO, A.; JANSSENS, P.; VANHOORNE, V.; VAN RENTERGHEM, J.; EECKHOUT, M.; CARDON, L.; DE BEER, T.; VERVAET, C. Screening of pharmaceutical polymers for extrusion-Based Additive Manufacturing of patient-tailored tablets. **International Journal of Pharmaceutics**, v. 586, p. 119591, 2020.

SEOANE-VIAÑO, I.; JANUSKAITE, P.; ALVAREZ-LORENZO, C.; BASIT, A. W.; GOYANES, A. Semi-solid extrusion 3D printing in drug delivery and biomedicine: Personalised solutions for healthcare challenges. **Journal of Controlled Release**, v. 332, p. 367–389, 2021.

SILVA, I. A.; LIMA, A. L.; GRATIERI, T.; GELFUSO, G. M.; SA-BARRETO, L. L.; CUNHA-FILHO, M. Compatibility and stability studies involving polymers used in fused deposition modeling 3D printing of medicines. **Journal of Pharmaceutical Analysis**, 2021.

TANG, Z.; FUJIMOTO, K.; OKAZAKI, S. All-atom molecular dynamics study of impact fracture of glassy polymers. II: Microscopic origins of stresses in elasticity, yielding, and strain hardening. **Polymer**, v. 207, p. 122908, 2020.

TEODORESCU, M.; BERCEA, M.; MORARIU, S. Biomaterials of PVA and PVP in medical and pharmaceutical applications: Perspectives and challenges. **Biotechnology Advances**, v. 37, n. 1, p. 109–131, 2019.

TRIYONO, J.; ALFIANSYAH, R.; SUKANTO, H.; ARIAWAN, D.; NUGROHO, Y. Fabrication and characterization of porous bone scaffold of bovine hydroxyapatite-glycerin by 3D printing technology. **Bioprinting**, v. 18, p. e00078, 2020.

VAROL, N.; DELPOUVE, N.; ARAUJO, S.; DOMENEK, S.; GUINAULT, A.; GOLOVCHAK, R.; INGRAM, A.; DELBREILH, L.; DARGENT, E. Amorphous rigidification and cooperativity drop in semi−crystalline plasticized polylactide. **Polymer**, v. 194, p. 122373, 2020.
.

WEI, Z.; WANG, R.; WANG, J.; YANG, Y.; LIU, Y.; WANG, W.; CAO, Y.. Highly toughened PA6 using residue of plasticized PVB film via two-step reactive melt blending. **Polymer**, v. 186, p. 102052, 2020.

WHO (WORLD HEALTH ORGANIZATION). The international Pharmacopoeia. Dept. of essential medicines and pharmaceutical policies. Uniformity of mass for single-dose preparations (5.2). 2019.

WONG, C. Y.; WONG, W. Y.; LOH, K. S.; MOHAMAD, A. B. Study of the plasticising effect on polymer and its development in fuel cell application. **Renewable and Sustainable Energy Reviews**, v. 79, p. 794–805, 2017.

XU, P.g; LI, J.; MEDA, A.; OSEI-YEBOAH, F.; PETERSON, M. L.; REPKA, M.; ZHAN, X.. Development of a quantitative method to evaluate the printability of filaments for fused deposition modeling 3D printing. **International Journal of Pharmaceutics**, v. 588, p. 119760, 2020. a.

XU, Y.; XU, Y.; SUN, C.; ZOU, L.; HE, J. The preparation and characterization of plasticized PVA fibres by a novel Glycerol/Pseudo Ionic Liquids system with melt spinning method. **European Polymer Journal**, v. 133, p. 109768, 2020. b.

YANG, Y.; WANG, H.; XU, X.; YANG, G. Strategies and mechanisms to improve the printability of pharmaceutical polymers Eudragit® EPO and Soluplus®. **International Journal of Pharmaceutics**, v. 599, p. 120410, 2021.

ZARE, Y.; RHEE, K. Y. Modeling of viscosity and complex modulus for poly (lactic acid)/poly (ethylene oxide)/carbon nanotubes nanocomposites assuming yield stress and network breaking time. **Composites Part B: Engineering**, v. 156, p. 100–107, 2019.

ZHANG, J.; FENG, X.; PATIL, H.; TIWARI, R. V.; REPKA, M. A. Coupling 3D printing with hot-melt extrusion to produce controlled-release tablets. **International Journal of Pharmaceutics**, v. 519, n. 1–2, p. 186–197, 2017.

ZI, B.; WANG, N.; QIAN, S.; BAO, K. Design, stiffness analysis and experimental study of a cable-driven parallel 3D printer. **Mechanism and Machine Theory**, v. 132, p. 207–222, 2019.